

Article

# InSAR Campaign Reveals Ongoing Displacement Trends at High Impact Sites of Thessaloniki and Chalkidiki, Greece

Nikos Svigkas <sup>1,\*</sup>, Constantinos Loupasakis <sup>2</sup>, Ioannis Papoutsis <sup>3</sup>,  
Charalampos (Haris) Kontoes <sup>3</sup>, Stavroula Alatza <sup>3</sup>, Ploutarchos Tzampoglou <sup>4</sup>,  
Cristiano Tolomei <sup>1</sup> and Thomas Spachos <sup>5</sup>

<sup>1</sup> Osservatorio Nazionale Terremoti, Istituto Nazionale di Geofisica e Vulcanologia, 00143 Rome, Italy; cristiano.tolomei@ingv.it

<sup>2</sup> Laboratory of Engineering Geology and Hydrogeology, Department of Geological Sciences, School of Mining and Metallurgical Engineering, National Technical University of Athens, 15780 Athens, Greece; cloupasakis@metal.ntua.gr

<sup>3</sup> Institute of Space Applications and Remote Sensing, National Observatory of Athens, 15236 Athens, Greece; ipapoutsis@noa.gr (I.P.); kontoes@noa.gr (C.K.); alatza@noa.gr (S.A.)

<sup>4</sup> Department of Civil and Environmental Engineering, School of Engineering, University of Cyprus, 1678 Nicosia, Cyprus; tzampoglou.ploutarchos@ucy.ac.cy

<sup>5</sup> Water Supply and Sewerage Company of Thessaloniki, 54635 Thessaloniki, Greece; spahos@eyath.gr

\* Correspondence: nikos.svigkas@ingv.it

Received: 19 June 2020; Accepted: 24 July 2020; Published: 26 July 2020



**Abstract:** We studied the broader area of Thessaloniki in northern Greece and Chalkidiki and performed an InSAR campaign to study the surface deformation phenomena that have been known to exist for at least two decades. Sentinel-1 data (2015–2019) together with drill measurements were exploited to focus on specific sites of interest. Our results indicate an ongoing displacement field. At the region of Kalochori and Sindos—where intense subsidence in the 1990s was previously found to have had a natural surface rebound in the 2000s—a new period of subsidence, caused by the enlivenment of the groundwater overexploitation, was reported. The uplifting trend of Oreokastro is still active and subsidence in Anthemountas graben is ongoing; special focus was set on the Makedonia Airport, where significant displacement is occurring. The study also reveals a new area at Nea Moudania, that was not known previously to deform; another case corresponding to anthropogenic-induced surface displacement. Thessaloniki is surrounded by different persistent displacement phenomena, whose main driving mechanisms are anthropogenic. The sensitivity of the surface displacements to the water trends is highlighted in parts of the study area. Results highlight the plan of a water resources management as a high priority for the area.

**Keywords:** InSAR; PSI time-series; deformation; Northern Greece; Kalochori; Oreokastro; Anthemountas; thessaloniki airport; Nea Moudania

## 1. Introduction

Thessaloniki is located in Northern Greece and is the second largest city of the country (Figure 1). Past studies of the broader area have highlighted several subsiding deformations occurring in the wider area (e.g., [1,2]). Synthetic Aperture Radar Interferometry (InSAR) techniques have been successfully applied using data from radar satellites for the monitoring of surface displacement in several cases globally (e.g., [3,4]) and also in Greece (e.g., [5–8]). The advent of technological advancements of radar satellites has provided significant input data and has given rise to a series of InSAR studies at the

wider region of Thessaloniki. Some of these studies have detected and measured the ground surface displacement (e.g., [9–11]). Other InSAR studies used in-situ data and ground campaigns to interpret and find the cause of the reported displacement signals [12–17]. It is widely accepted that underground water activity can cause surface displacement [18]. This paper aims to study the surface deformation occurring in the vicinity of Thessaloniki (Figure 1) and to consider the role of anthropogenic activities in the evolution of these deformation phenomena. Aquifer overpumping had been identified as the main cause of deformation for the areas of Kalochori–Sindos, for the broader area of Oreokastro, as well as for the Anthemountas basin (Figure 1) [12–17].

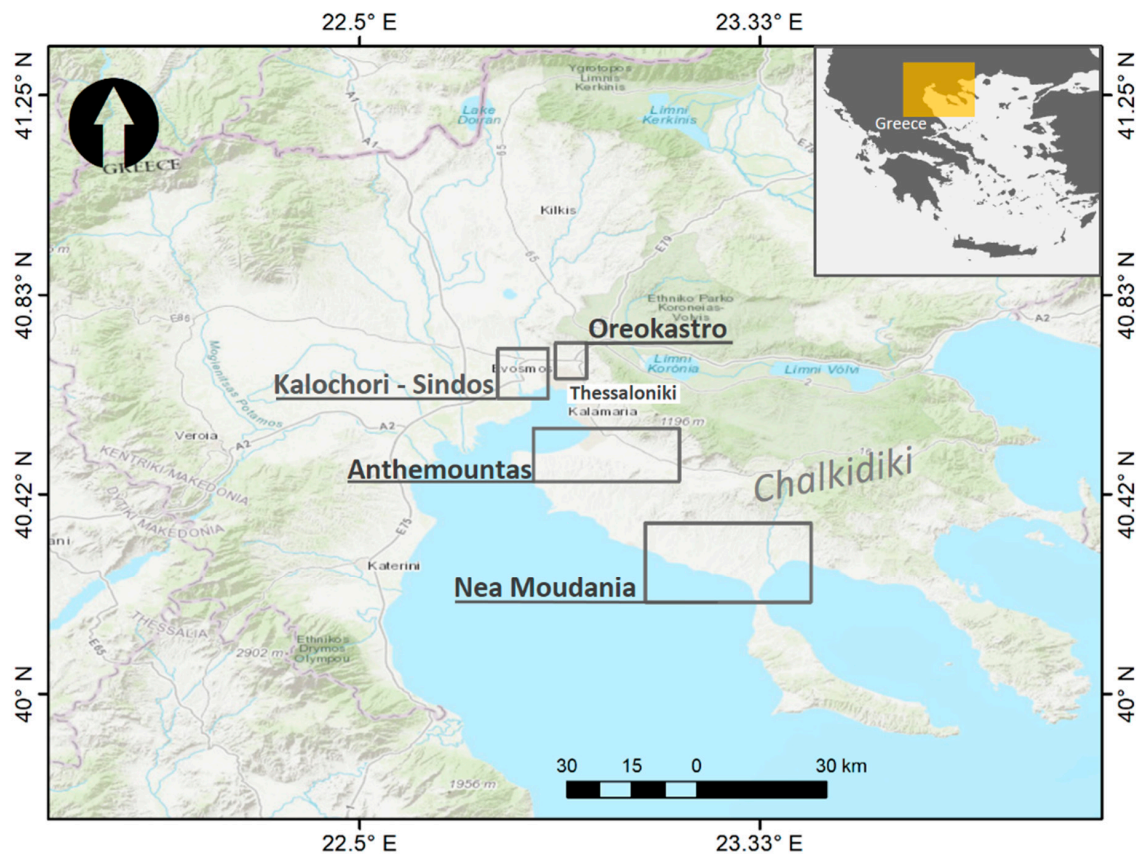


**Figure 1.** Areas of interest in Northern Greece located in the wider Thessaloniki and Chalkidiki regions. Orange rectangle in the upper inset map indicates the broader study site. The areas have been studied in the framework of the Greece InSAR project run by NOA/BEYOND ([www.beyond-eocenter.eu](http://www.beyond-eocenter.eu)) using Sentinel-1 data of the period 2015–2019.

In this study, we exploit the Sentinel-1 satellite, operated by the European Space Agency (ESA), to answer the question of whether there is a considerable continuing, persisting hazard at the sites of interest or whether it has diminished or been replaced by other types of geo-hazards. The geo-hazard interpretation is strongly supported by using data from in-situ conducted campaigns in the specific sites of interest. Focus is set on the areas of Kalochori–Sindos, Oreokastro, and Anthemountas, which were highly impacted by surface displacement, the latter resulting occasionally in numerous damages of houses, roads, and industrial buildings. Moreover, new deformation evidence has emerged at the area of Nea Moudania (Figure 1). No previous study has reported any type of deformation occurring in this area. Apart from the scientific curiosity that is the dominant driver for the study, significant motivation has also been the fact that the broader Thessaloniki metropolitan area consists a hub for the Balkans and south-eastern Europe; here lay important economic activities and critical infrastructure, and many actors are placed belonging to the primary and touristic sectors as well.

## 2. Methods and Data Used

We used 91 Sentinel-1 satellite images, descending pass, orbit no. 7, and frame 457, spanning the period 12 December 2015–15 December 2015 (Table 1). The detection and measurement of surface displacement was achieved by performing Multi Temporal InSAR (MT-InSAR). Our processing chain was Parallelized Persistent Scatterer Interferometry (P-PSI; Papoutsis et al. [19]) which is a novel, distributed processor for the fully automated and computationally efficient assessment of line-of-sight ground velocities through PSI, tailored to scale to the large multi-temporal archive of Sentinel-1 data.

**Table 1.** Radar data used.

| Date            | Normal Baseline | Date            | Normal Baseline | Date            | Normal Baseline |
|-----------------|-----------------|-----------------|-----------------|-----------------|-----------------|
| 12 December 15  | −88             | 28 February 17  | 37              | 26 November 18  | 15              |
| 24 December 15  | 6               | 12 March 17     | −15             | 08 December 18  | −38             |
| 05 January 16   | 48              | 24 March 17     | 84              | 20 December 18  | 47              |
| 17 January 16   | 94              | 05 April 17     | 77              | 01 January 19   | 45              |
| 29 January 16   | 89              | 17 April 17     | 75              | 13 January 19   | 75              |
| 10 February 16  | 7               | 29 April 17     | 49              | 06 February 19  | 19              |
| 05 March 16     | 33              | 11 May 17       | −26             | 02 March 19     | −19             |
| 17 March 16     | 112             | 20 October 17   | 0               | 14 March 19     | 117             |
| 29 March 16     | 65              | 01 November 17  | −14             | 26 March 19     | 58              |
| 10 April 16     | 35              | 13 November 17  | 53              | 07 April 19     | −5              |
| 22 April 16     | 5               | 25 November 17  | 45              | 19 April 19     | −40             |
| 16 May 16       | 73              | 07 December 17  | 37              | 01 May 19       | −40             |
| 28 May 16       | 78              | 19 December 17  | −51             | 13 May 19       | 98              |
| 09 June 16      | 73              | 31 December 17  | −31             | 06 June 19      | 61              |
| 15 July 16      | 95              | 05 February 18  | 30              | 18 June 19      | 58              |
| 27 July 16      | 103             | 01 March 18     | −15             | 30 June 19      | 16              |
| 08 August 16    | 59              | 11 June 18      | 18              | 12 July 19      | 86              |
| 20 August 16    | −12             | 23 June 18      | 62              | 24 July 19      | 98              |
| 01 September 16 | 81              | 05 July 18      | 163             | 05 August 19    | 82              |
| 13 September 16 | 61              | 17 July 18      | 85              | 17 August 19    | −25             |
| 25 September 16 | 23              | 29 July 18      | 77              | 29 August 19    | 27              |
| 07 October 16   | 33              | 10 August 18    | 24              | 10 September 19 | 81              |
| 19 October 16   | 66              | 22 August 18    | 116             | 22 September 19 | 48              |
| 31 October 16   | −36             | 03 September 18 | 44              | 04 October 19   | 17              |
| 12 November 16  | 36              | 15 September 18 | 71              | 16 October 19   | 46              |
| 24 November 16  | 40              | 27 September 18 | 23              | 28 October 19   | 31              |
| 06 December 16  | 22              | 09 October 18   | 19              | 09 November 19  | 36              |
| 11 January 17   | −30             | 21 October 18   | 34              | 21 November 19  | 68              |
| 23 January 17   | 68              | 02 November 18  | 49              | 03 December 19  | 44              |
| 04 February 17  | 68              | 14 November 18  | 15              | 15 December 19  | −29             |
| 16 February 17  | 86              |                 |                 |                 |                 |

Our P-PSI implementation invokes two main software packages that have been modified to parallelize the execution of the different processing tasks. We use the InSAR Scientific Computing Environment (ISCE) with the topsStack processor [20] for creating a stack of coregistered Single Look Complex (SLC) datasets. Several processing steps with ISCE software were parallelized, including the generation of overlap interferograms and the computation of geometrical offsets among all slave SLCs and the stack master, for precise coregistration. The SLC stack was then used for PSI analysis with a parallelized implementation of the Stanford Method for Persistent Scatterers (StaMPS; Hooper et al. [21,22]), a process that produces ground velocities and deformation histories for the Persistent Scatterers (PS) that have been detected. The full Sentinel-1 frame was divided in sub-regions, i.e., “patches”. Our processing chain exploited multi-core programming techniques to execute simultaneously the processing steps of the Stanford method for Persistent Scatterers in multiple

patches. StaMPS relies on the spatial correlation of the deformation, rather than on a temporal linear deformation model. It is therefore suitable to also detect non-linear deformation.

To estimate the topography effect, the Shuttle Radar Topography Mission Digital Elevation Model (SRTM DEM) [23] with a resolution of 1 arc-second, was employed. In order to have a reasonable trade-off between a larger pixel spacing and pixels with random phase, we opted for a threshold of 20 m for the maximum topographic error. To exclude pixels considered as “noisy” or pixels selected as PSI, due to signal contribution from neighboring ground resolution elements, a threshold of 1 was selected for the phase noise standard deviation for all pixel pairs. Therefore, pixels exceeding this threshold were excluded from further steps of PS processing.

The open-source Toolbox for Reducing Atmospheric InSAR Noise (TRAIN) [24] was employed, by implementing a phase-based linear correction on interferograms produced for PS processing. Since the areas of interest investigated are characterized by divergent topography, the linear correction applied, which compensates for the tropospheric delay relative to the topography, provides a satisfying accuracy in the tropospheric delay correction.

The outcome of P-PSI is a collection of pixels (PS) with stable phase over time. These points provide estimates of annual velocities and a quality measure named velocity standard deviation (Figure S1). High values for the latter indicate either a noisy estimate or provide an indication of non-linear deformation. In addition, for each PS, a deformation time-series in the period 2015–2019 was provided that highlights various deformation trends.

### 3. Results

The interferometric pairs that were formed are schematically shown in Figure 2 with respect to their temporal and perpendicular baselines. We processed the entire set of available Sentinel-1 images for the area and period of interest and identified a dense and spatially well distributed network of 1,551,817 stable-phase pixels, for which we estimated ground displacements (Figure 3).

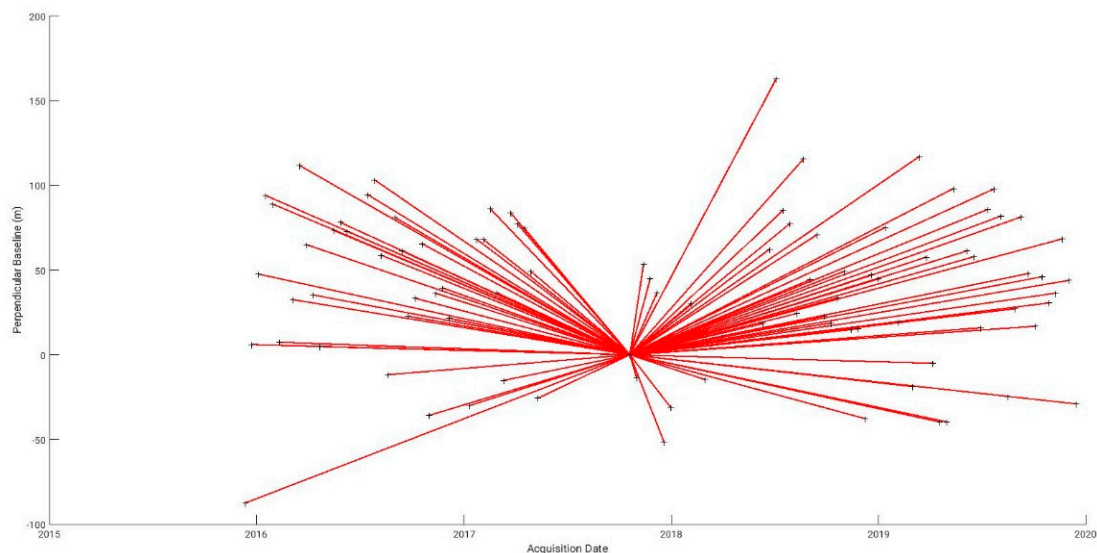


**Figure 2.** Sentinel-1 SAR imagery PSI connection graph. The date of the master SAR scene used for PSI analysis was 20 October 2017. Perpendicular baselines are confined within  $\pm 150$  m only, given the short Sentinel-1 orbital tube.

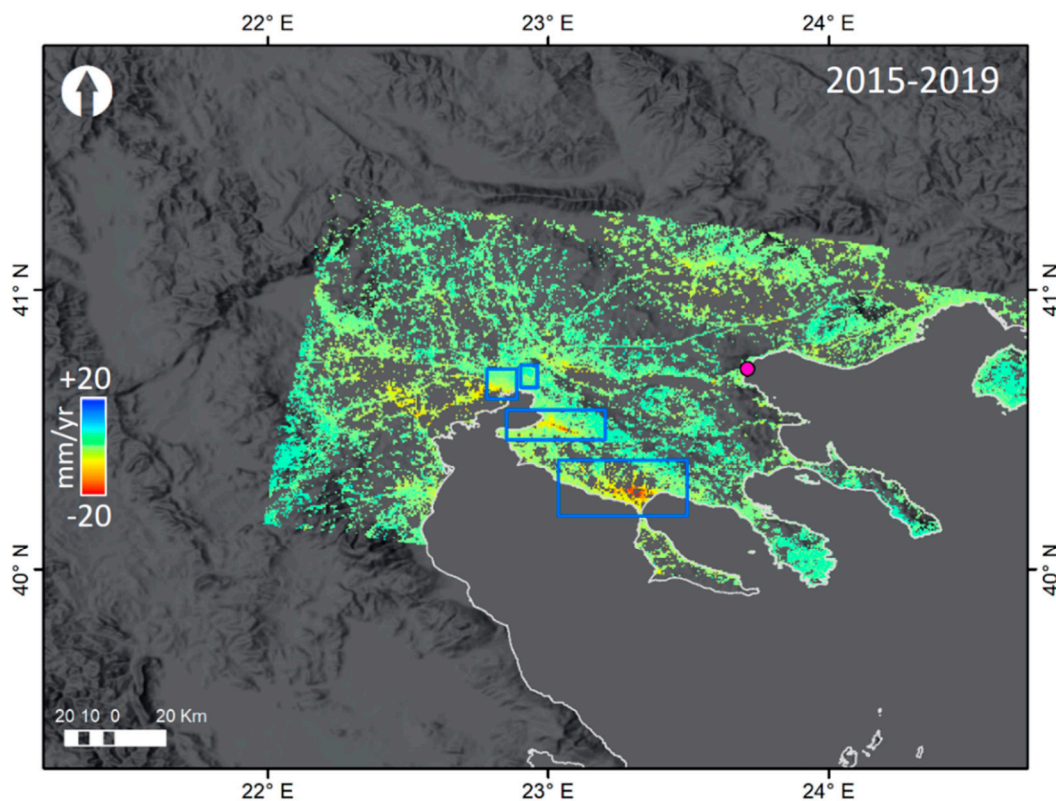


**Figure 3.** Sentinel-1 PS LoS velocity results in Northern Greece, for the period 2015–2019. Blue rectangles indicate the areas of study (see also Figure 1). The magenta dot indicates the VRAS c-GPS stations used as a reference point for the processing of the specific Sentinel-1 frame.

Since PSI estimates are a relative measurement on both the spatial and temporal domain, we used in our PSI the SAR acquisition of 20 October 2017 as the master scene for temporal reference, and the VRAS continuous GPS station (Figure 3) as a spatial reference point. VRAS has data for four years in the period 2013–2016, is 80 km away from Thessaloniki, and is located in an area for which there is no prior evidence that it has been deforming. VRAS data shows that movement in the Up direction is negligible ( $\sim 0.1$  mm/yr) with some seasonal movement, as expected. The stability of the VRAS station ensures us that we do not need to take account of a constant bias in our velocities estimations.

The results indicate that there is surface deformation at the areas of interest, enclosed by the blue rectangles shown in Figure 3. More specifically in the area of Kalochori–Sindos there is a subsidence signal, Oreokastro has an uplifting trend while a subsidence trend appears to exist at the basin of Anthemountas. A new area not previously known to deform is the Nea Moudania plain (Figures 1 and 3).

The following sections focus on each of these areas, analyze the findings from InSAR processing and ground truth data when available, and attempt to provide interpretations on the reported signals.

### 3.1. Kalochori–Sindos Region

The villages of Kalochori and Sindos are located at the west of Thessaloniki (Figure 1). The area is known for the intense industrial activity. It is located on Quaternary deposits (Figure 4) with the sediments consisting of sands, clays, and silty clays [25,26]. The upper 5 to 15 m of the Quaternary deposits are occupied by fine-to-medium grained sand intercalated by silty sand horizons. Underneath, a 25 to 35 m thick black-grey silty sand horizon with organic materials extends, forming an impermeable boundary, determinant for the hydrogeological conditions of the site. The lower strata, down to the Neogene bedrock, consist of alternating brown sand and black-grey silty sand horizons [26,27].

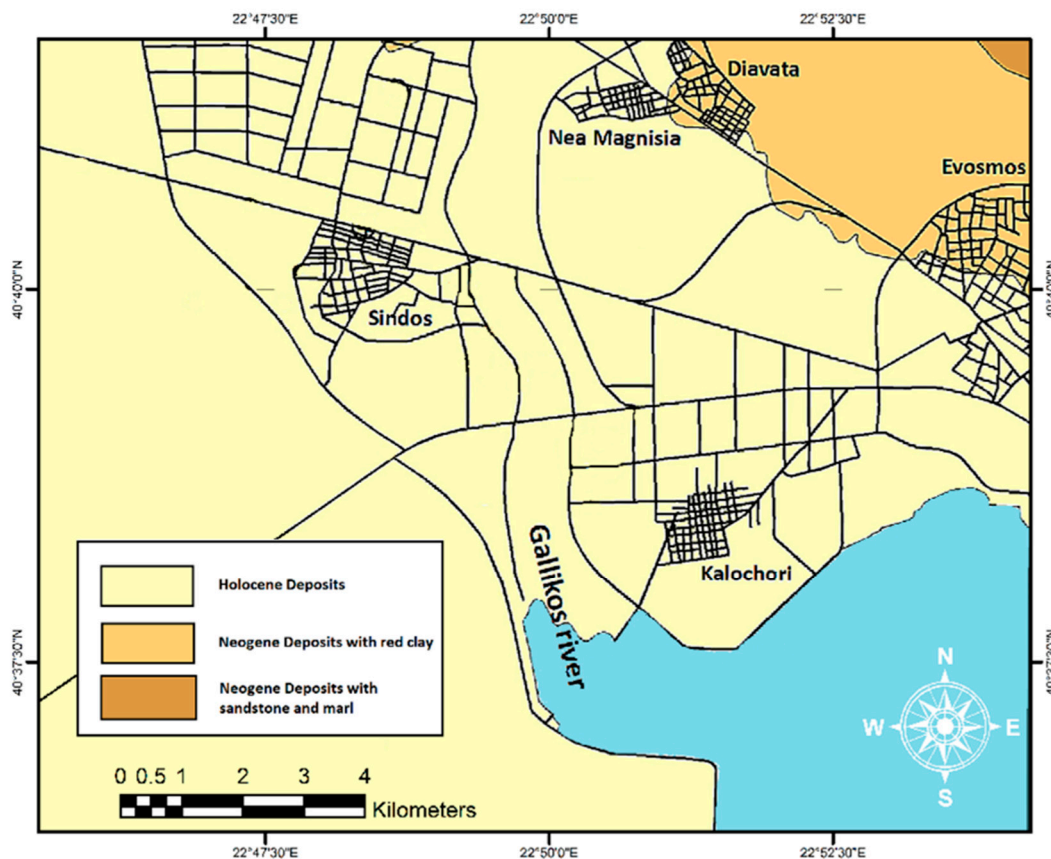


**Figure 4.** Geological map of the broader area of Kalochori–Sindos, source: [28] and [13] (modified from [14]).

From a hydrogeological point of view, two aquifers can be identified: a shallow aquifer unconfined within the sandy layer of the upper strata, and a deeper confined aquifer system within the brown sand of the lower strata. The quality of the water of the shallow aquifer is poor, in contrast to the high quality water of the second confined aquifer system, extending below the impermeable organic silty sand horizon. The overexploitation of the confined aquifer has been proven as the main cause of the land subsidence phenomenon occurring at the site.

Ground truth techniques had been used to study the subsiding pattern that was known since the 1960s [25,29–32]. The 1990s InSAR displacement was first identified by Raucoules et al. [10] using acquisitions from the European Remote sensing Satellite (ERS) satellites. A detailed investigation by Raspini et al. [13] used the ERS satellite results (1990s dataset), together with in-situ data for the interpretation of the detected subsidence. However, in a later study, an uplifting pattern was identified in Svigkas et al. [11] corresponding to the post-2000 period, covering the Environmental Satellite (ENVISAT) satellite era. This change in the deformation trend was attributed to the natural recharge of the aquifers, due to the cessation of groundwater pumping [14]. A Global Navigation Satellite System (GNSS) study covering the period 2013–2015 showed a mixture of subsidence and uplift displacement pattern [33].

The Sentinel-1 interferometric results presented in Figure 5 indicate that the uplifting trend of the 2000s has been reversed again and now a new period of subsidence is occurring in the area. Maximum displacement values in the vicinity of Kalochori are of the order of  $-10$  mm/yr, while in the broader area, maximum values reach a rate of  $-14$  mm/yr.

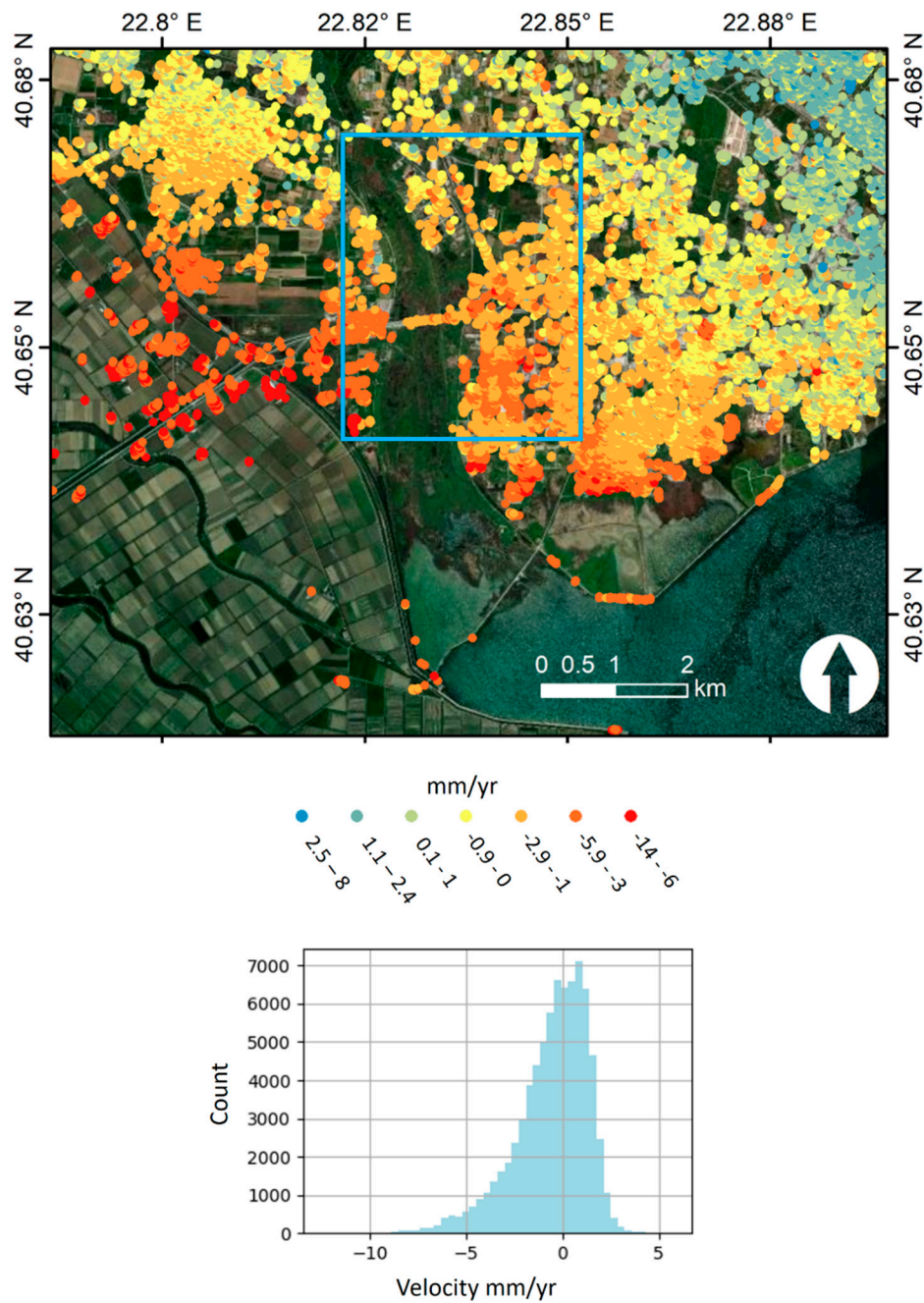


**Figure 5.** PSI ground velocity results for Kalochori-Sindos as derived from the Sentinel-1 PSI analysis. Blue rectangle is the area shown also in Figure 6 (inset map) and Figure 7. The histogram at the bottom row highlights the prevailing subsidence trend in the region.

Hydrogeological data of the region enabled the validation and interpretation of the PSI Sentinel-1 based results. The drill data of the same period indicate a decrease in the underground water levels (Figure 6), which in most drills appears to have been initiated between 2016 and 2017. The amount of dropdown from November 2015 to November 2019 agrees spatially with the areas of significant displacement (Figure 7) depicted by the PSI processing.

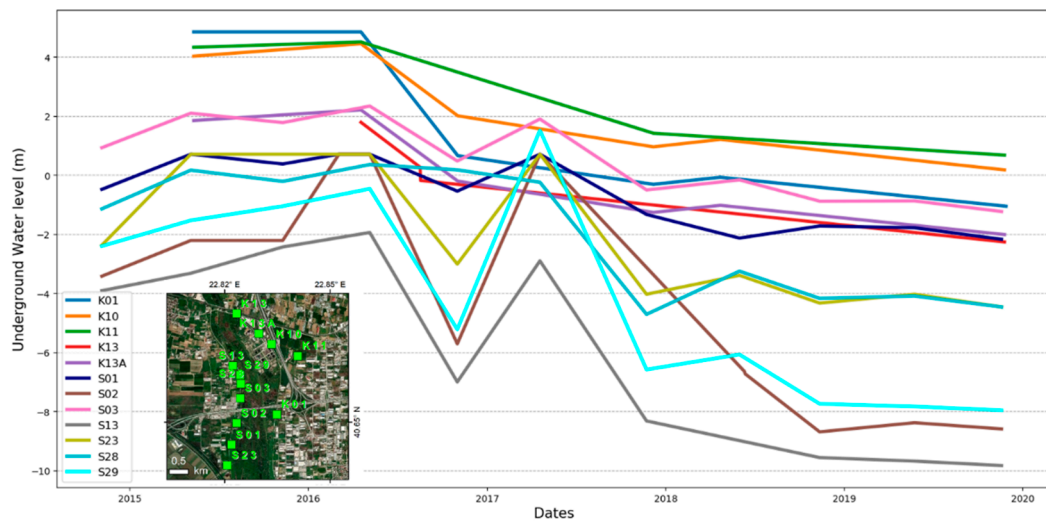


**Figure 6.** In-situ underground water level measurements conducted during the Sentinel-1 PSI monitoring period. The green rectangles in the inset map are the locations of the drills; the area of the inset map is shown in the blue rectangle of Figure 5.

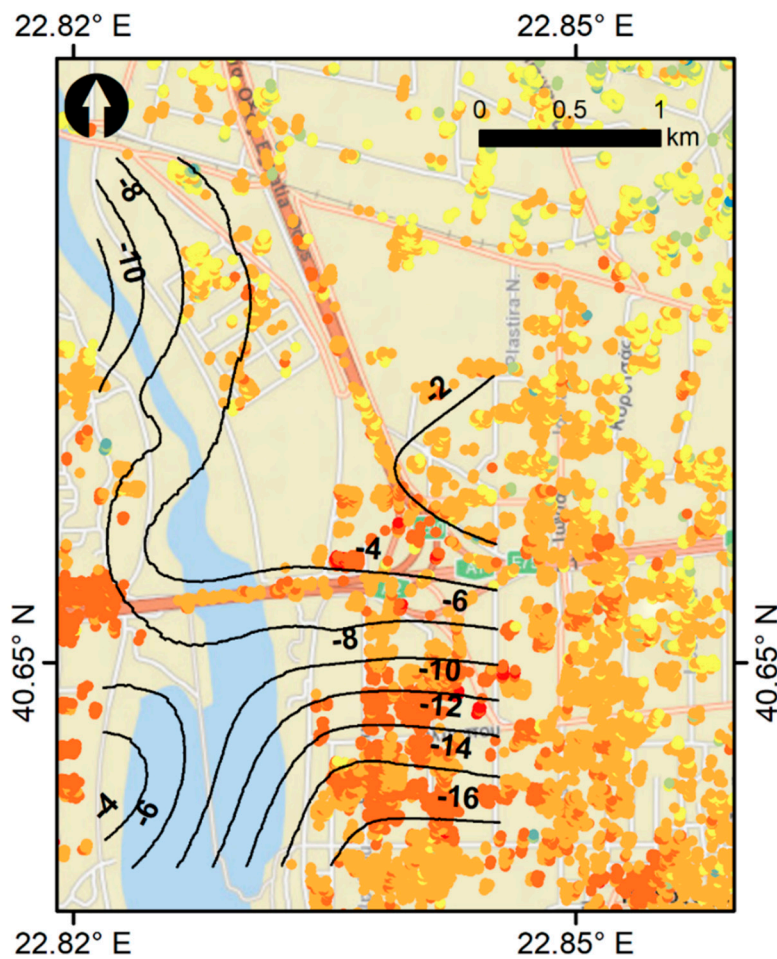


**Figure 7.** Underground water level changes of the deep confined aquifer between November 2019–November 2015 at the broader area of Kalochori. This is a zoom of the area; its extent is shown with the blue rectangle in Figure 5.



In order to have a holistic and temporally complete view of the phenomenon that has been occurring at Kalochori over the last decades, a graph presenting the groundwater level of a drill, together with the surface deformation estimated at the exact neighborhood of that drill, is presented in Figure 8. The plot shows that the subsidence taking place during the 1990s was followed by a rise of the hydraulic head—due to natural rebound—which in turn resulted in a surface uplift the following years [14]. The current analysis of satellite and in-situ hydrogeology data, indicates a potential onset of a new cycle of subsidence, derived from the recent downward trend of the aquifer water level (Figure 8). The subsidence trend of Sentinel-1 SAR results appeared with a time-lag of  $\sim 2$  years with respect to the initiation of the lowering of the hydraulic head. Similarly a  $\sim 2$ -year time-lag had been also identified at all former changes of the trend of the curves; namely when the aquifer started to recover and when the recovery trend was reduced during 2006 (Figure 8).



**Figure 8.** PSI based surface displacement vs. in-situ underground water level. Older data, corresponding to the period 1990–2014, were derived from the interferometric processing of ERS and ENVISAT data as well as in-situ water level measurements as reported in [14]. Whenever there is a trend change in the underground water level, surface deformation follows this change with an approximate time-lag of two years.

### 3.2. Oreokastro Industrial Zone

Oreokastro is located at the exact proximity of Thessaloniki (Figure 1) and is an area strongly related with the industrial activities of the city. The town was founded on a Pliocene lake and fluvial deposits. The industrial zone of Oreokastro is on Pliocene clays intercalated by sand, lying above the Pre-Alpine bedrock (Figures 9 and 10). The main tectonic features are the Efkarpia fault and the Asvestochori fault, both considered as potentially active [34]. No major seismic event is known to exist and the area is mainly related with microseismicity [35–37].

InSAR techniques had previously revealed that the area has been deforming [10]. The subsidence of the 1990s was followed by an uplifting trend after 2000. In Svigkas et al. [15], by combining remote sensing analysis with seismological, geological, and hydrogeological data of the area, it was shown that the observed displacement—which also caused building failures—was related with the activity of aquifers. Also, the displacement was found to be a fault-controlled pattern, in a sense that the faults at the area were most likely acting like water-flow barriers.

Sentinel-1 PSI results indicate a continuation of the uplifting pattern (Figure 11), previously detected to occur during the 2002–2010 ENVISAT based monitoring period. Specifically, the maximum uplifting rate was found to be as high as 8 mm/yr, which is essentially the same order of value as the one observed during the ENVISAT era (9 mm/yr).

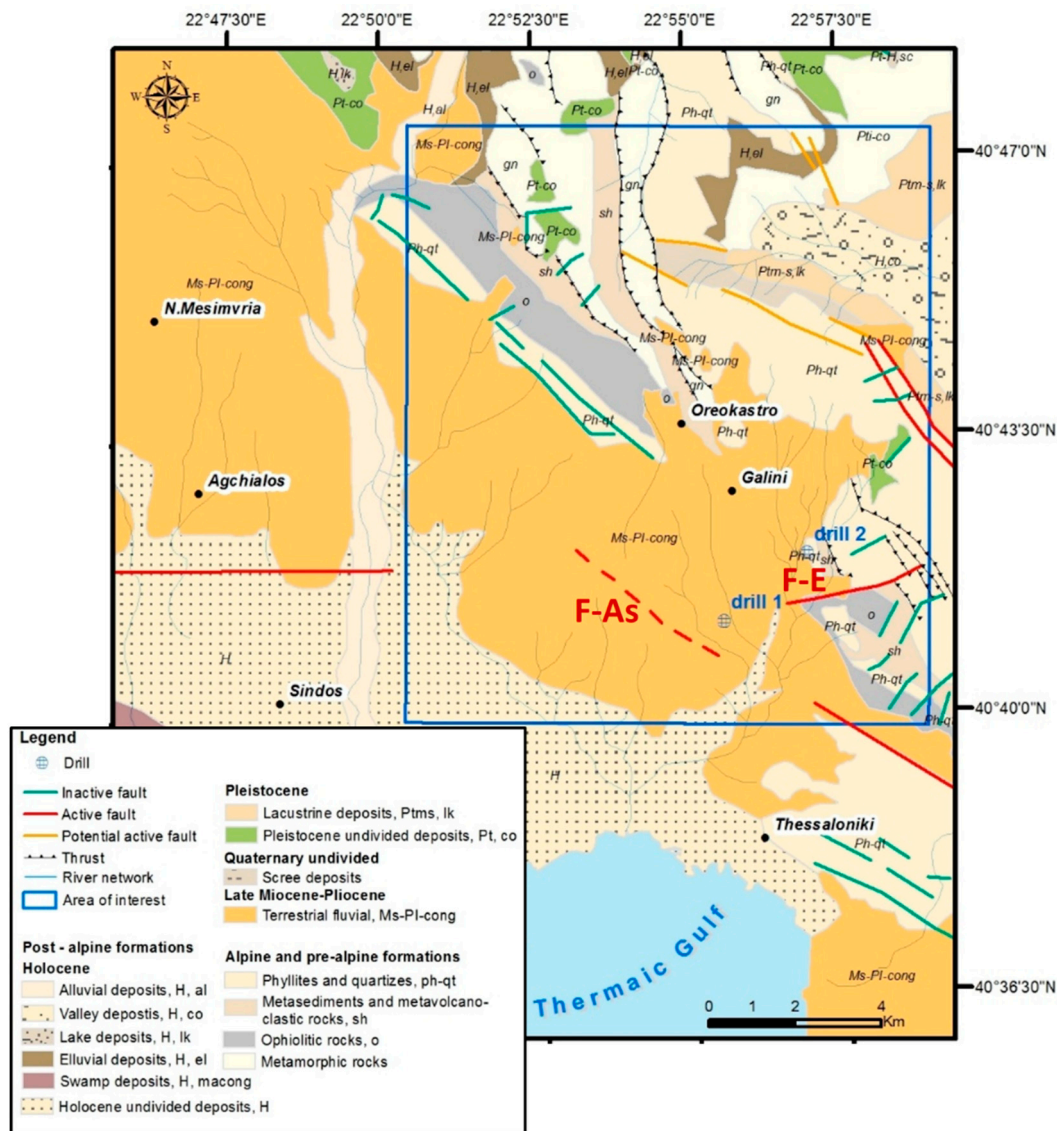


**Figure 9.** The geology of the broader area of Oreokastro (blue rectangle). Main tectonic features are the Asvestochori fault (F-As) and the Efkarpia fault (F-E). Drill data are shown in Figure 10, source: [38] (modified from [15]).

To analyze with higher detail the displacement pattern, velocity profiles were created (Figure 12). It can be seen that in all the profiles under study that the Asvestochori fault (Figure 9) is affecting the displacement trend.

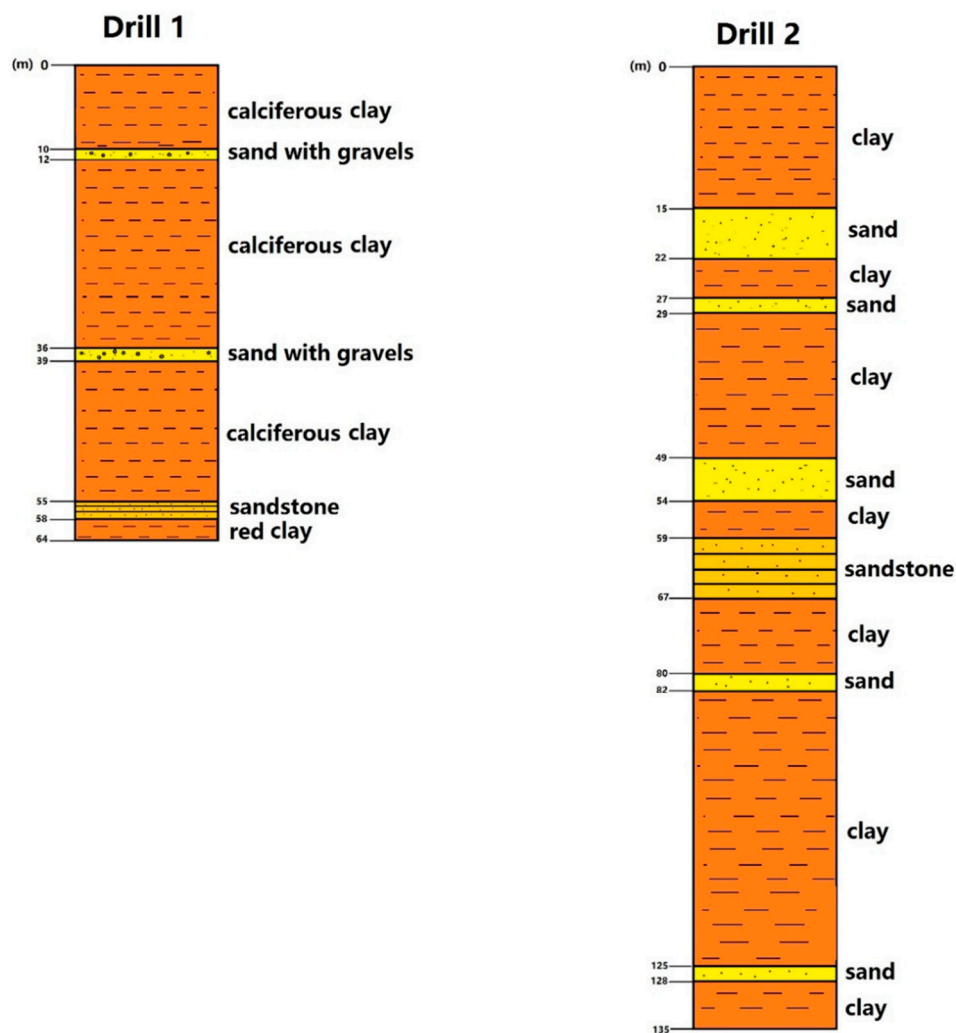


**Figure 10.** Stratigraphy of the broader area of Oreokastro (Figure 9). Borehole data are archives of the Directory of Environment, Thessaloniki Prefecture (modified from [15]).

Based on the ENVISAT results, Svigkas et al. [15] proposed that at the area there is an unknown feature highlighted by abrupt changes in the deformation trends. The interferometric analysis conducted showed that between the uplifting pattern and the Asvestochori fault, there was a thin subsiding zone just north of the fault and before the expression of the uplift. The same pattern appears also in the present study (Figure 11) of the Sentinel-1 based interferometric processing. However this time the deformation pattern presents a slightly different geometry than the one of the period 2003–2010, a phenomenon that might be related to the difference of underground water level activity, during the two monitoring periods. An explanation for this could be the different amounts of the underground water level uprising that might cause a different surface displacement pattern, depending also on the various permeabilities of the earth strata that the water flow meets.

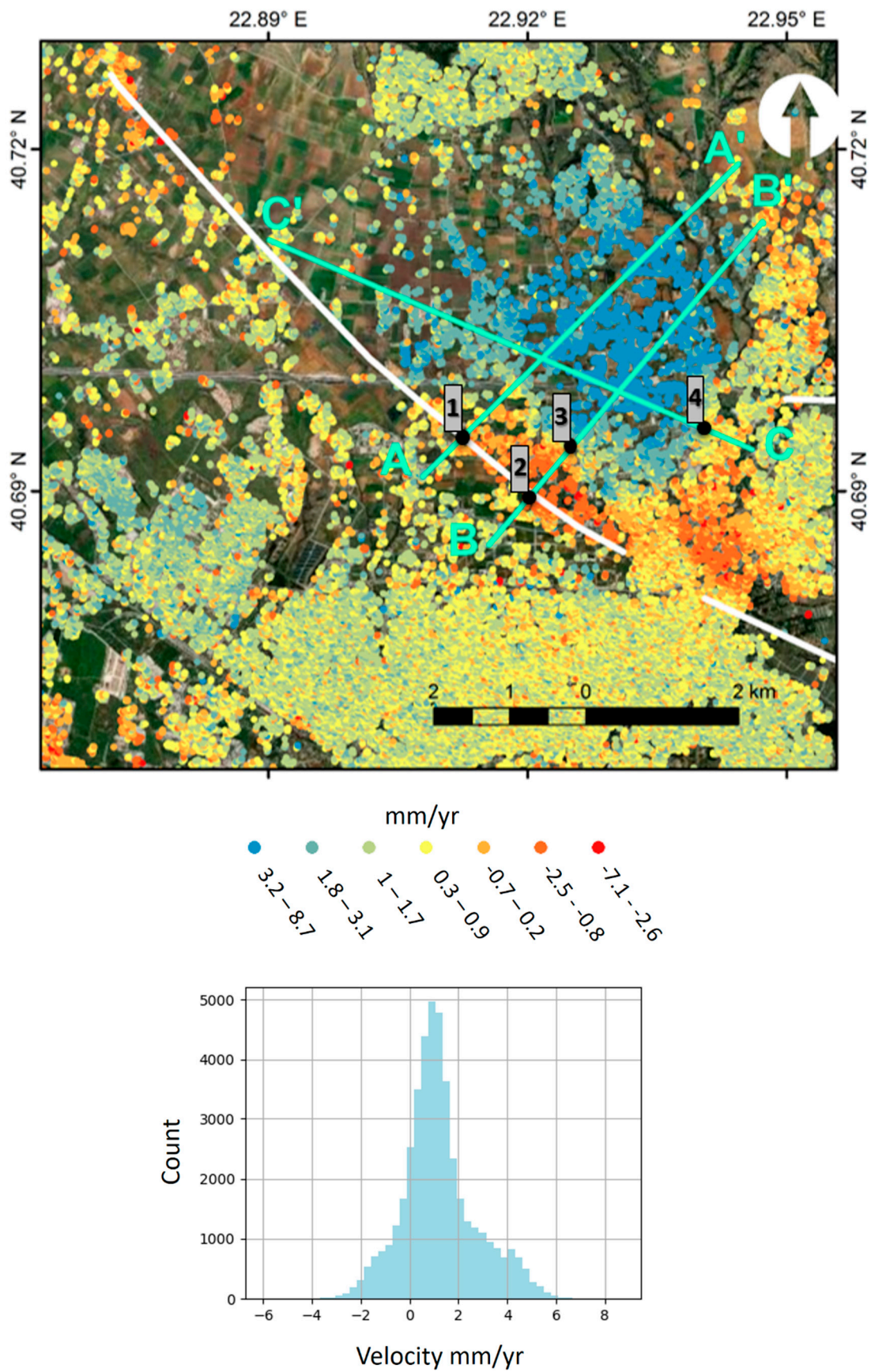


**Figure 11.** PS velocities of the broader area of Oreokastro. Green lines are velocity profiles presented in Figure 12. AA', BB', and CC' and numbers 1–4 are velocity profiles and points of interest respectively, noted also in Figure 12. Faults are from the National Observatory of Athens (NOA) fault database [39].

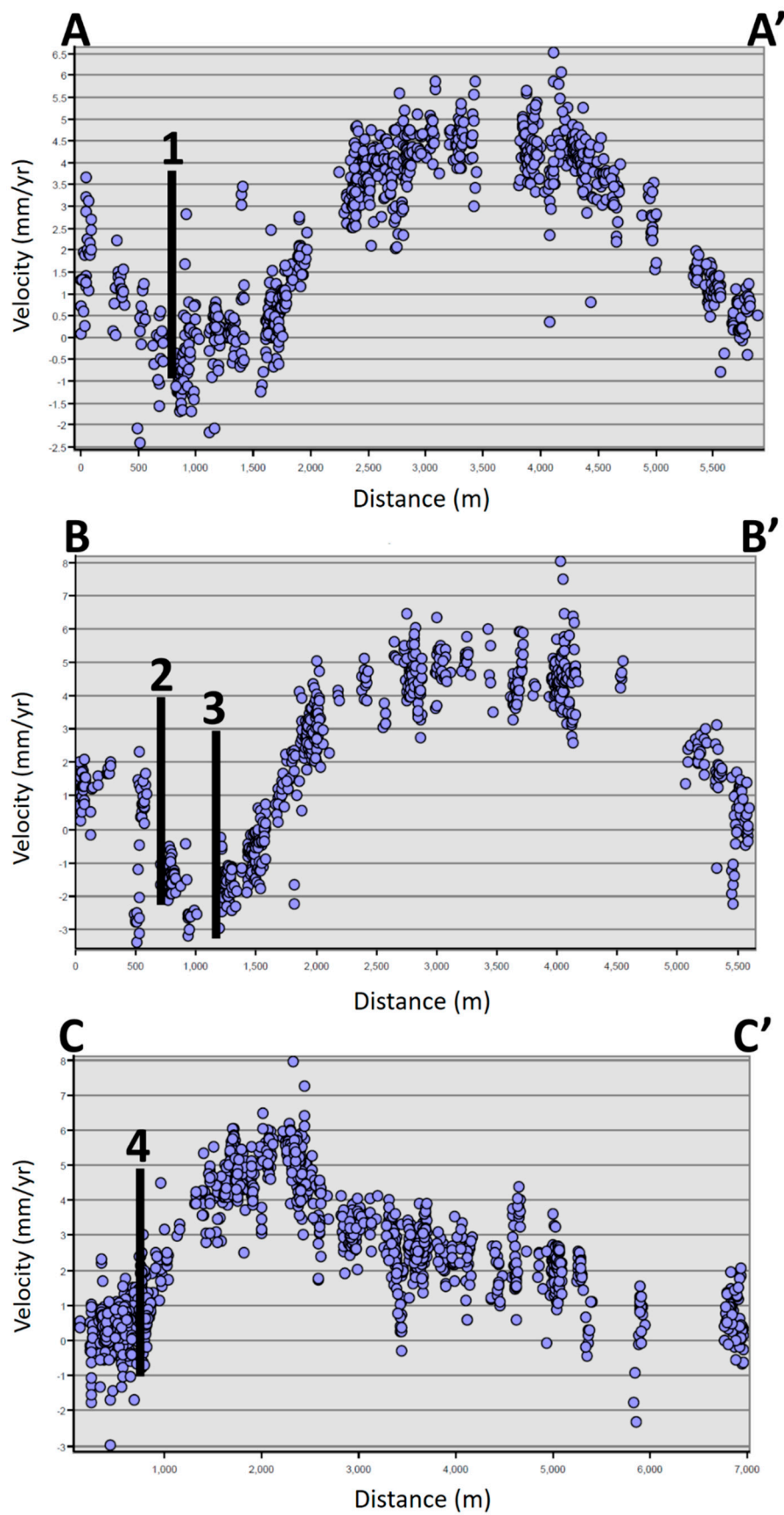


**Figure 12.** Velocity profiles in Oreokastro. Vertical black lines 1 and 2 in AA' and BB' respectively indicate locations attributed to the Asvestochori fault. Vertical Lines 3 and 4 in profile BB' and CC' respectively mark terminations of the Oreokastro uplifting displacement pattern.

### 3.3. Anthemountas Basin

Anthemountas basin is located west of the city of Thessaloniki (Figure 1). In the area the development trends had already started before the 1990s [40]. Here lay the longest tectonic structures close to the city of Thessaloniki; the northern branch of Anthemountas fault (F1 in Figure 14) that has a length of 21 km, considered inactive [34], and the south branch of Anthemountas fault (F-2). Morphotectonic studies indicate it as being an active fault structure [34,41].

Regarding the geological structure of the site, the top Quaternary formations consist of alterations of clastic and fine sediment [34,42,43]. At the Quaternary deposits (Figures 13 and 14), three main horizons can be identified: a) coarse to fine sand b) clay to silty clay horizon, and c) Neogene deposits characterized by coarse to fine sands. The Neogene deposits consist of a top sand and gravel layer and a bottom clay-marl layer [42,44]. The area has a Mesozoic bedrock where phillites, gneiss, and granites lie. The thickness of the sediments decreases when moving towards the east.

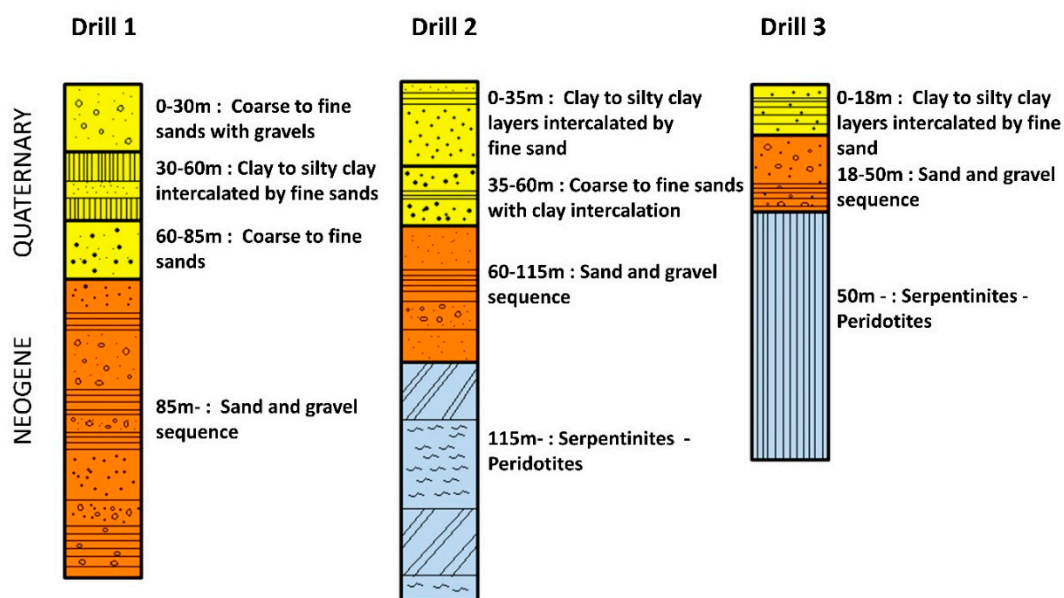


Figure 13. Borehole data of Anthemountas basin, source: [12] (modified from [17]).

In the upper strata of the Quaternary deposits, there is a shallow aquifer system interacting with a deeper semi-confined aquifer extending down to the Neogene formations [45]. The water demands of the area have caused a decrease of the groundwater level.

Raucoules et al. [10] used acquisitions of ERS satellites and by applying InSAR time-series detected subsidence during the 1990s. It was found that the displacements were extending from the coastal zone of the graben throughout the entire structure, up to the far East of the basin [16]. Raspini et al. [12] attributed the subsidence phenomena of the 1990s—that appeared to have also caused building failures—to aquifer overpumping. The subsidence in Anthemountas continued after 2000 and had been occurring continuously and increasingly for at least 20 years [17].

The observations based on PSI processing of Sentinel-1 images are presented in this study and indicate that the subsidence phenomenon is still active (Figure 15). The maximum subsidence value at the site appears to be  $-18$  mm/yr, the same as the maximum values previously detected during the ENVISAT imagery era [17]. Detailed velocity profiles are shown in Figure 17.

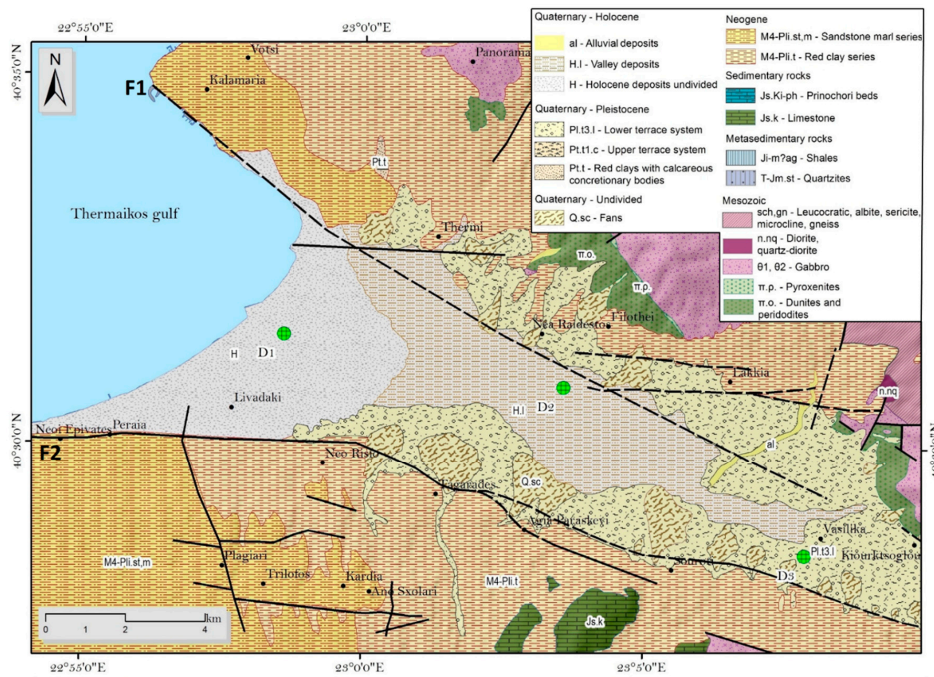


Figure 14. Geological map of Anthemountas graben, source: [46] (modified from [17]).

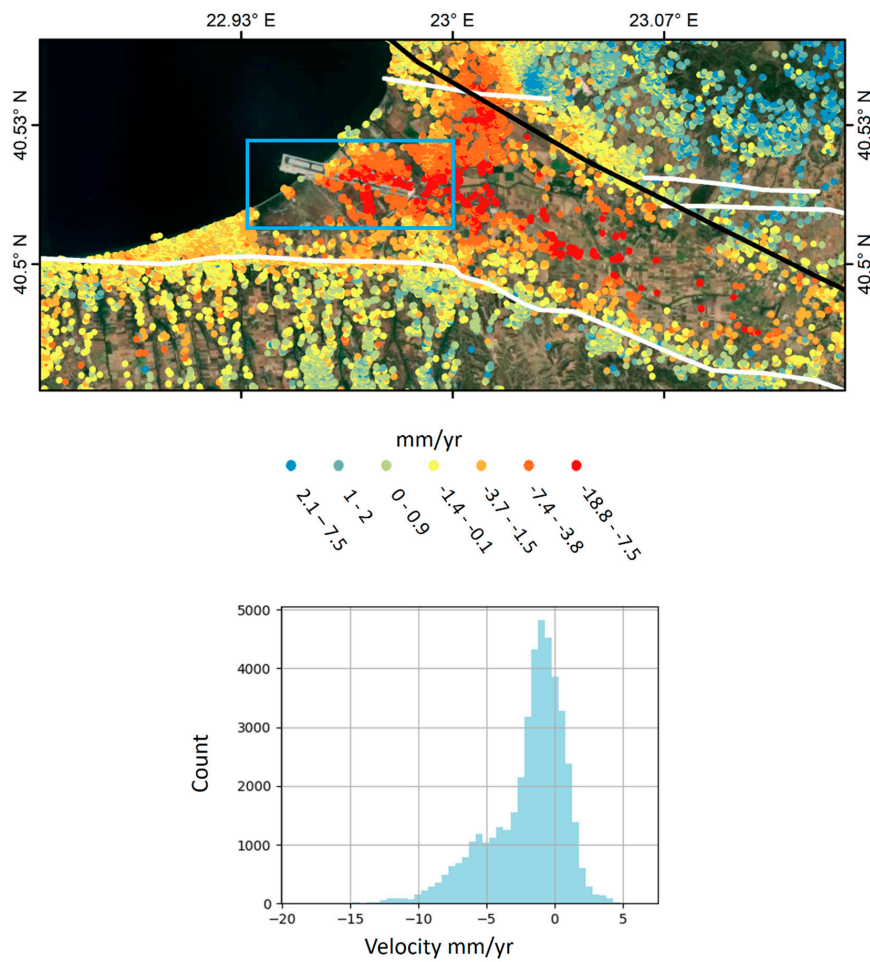
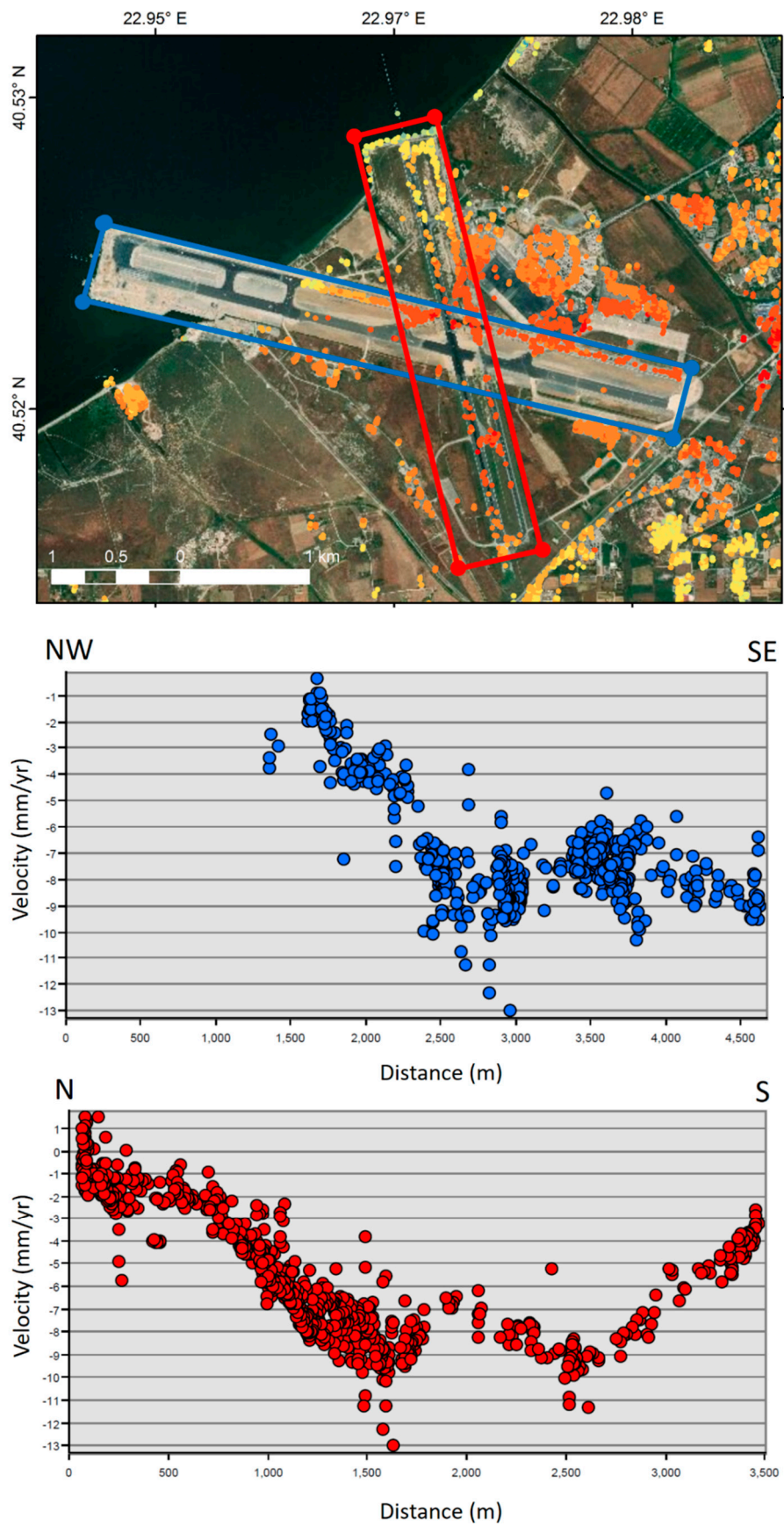


Figure 15. Velocity results for the Anthemountas graben. Cyan rectangle indicates the location of the Makedonia International Airport (Figure 16).



**Figure 16.** PS Sentinel-1 results of the Makedonia International Airport. Graphs are velocity profiles of the two runways. Blue profile swath shown in the map is shown at the top graph, red profile swath of the map is shown at the bottom graph.



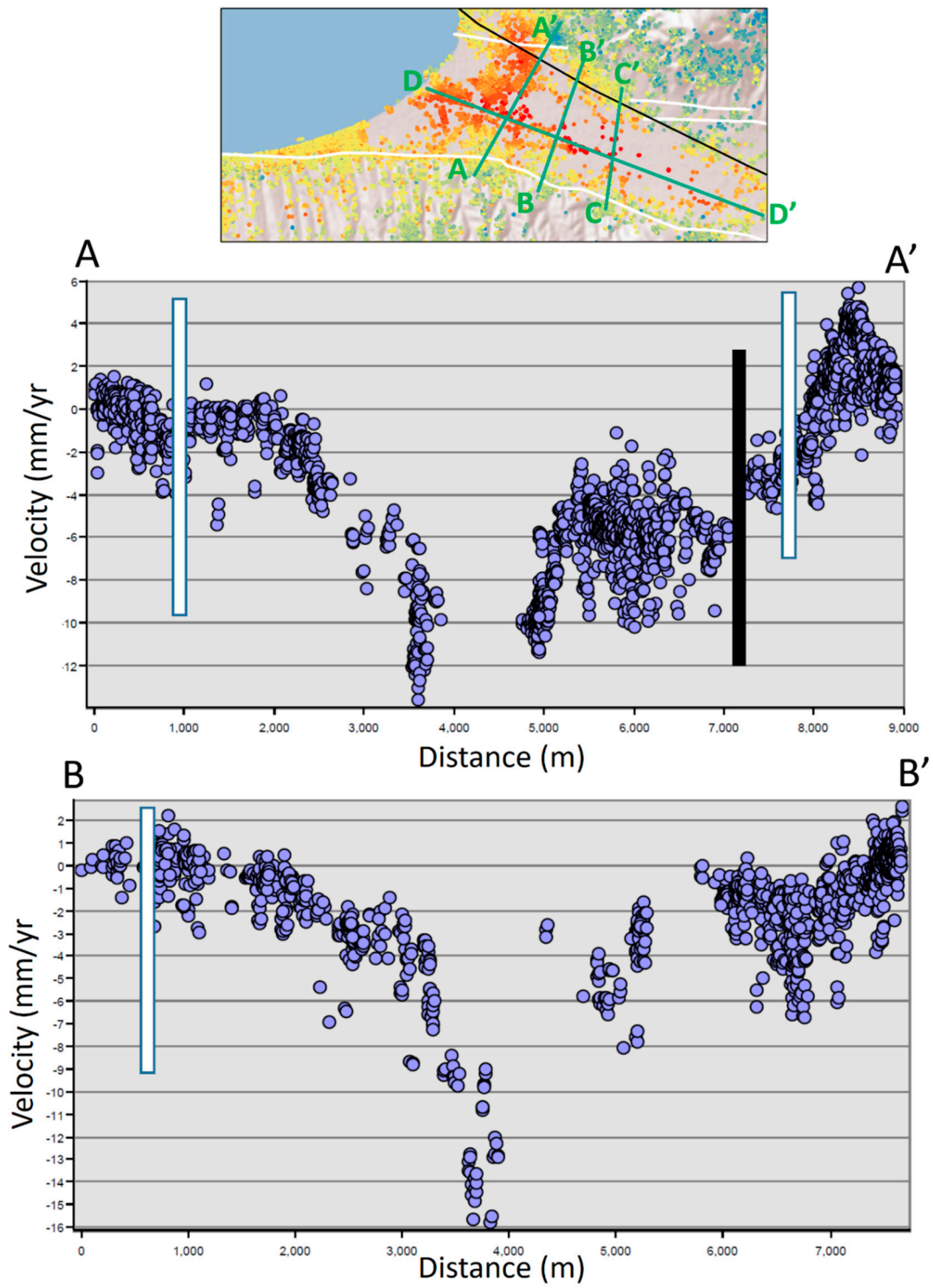
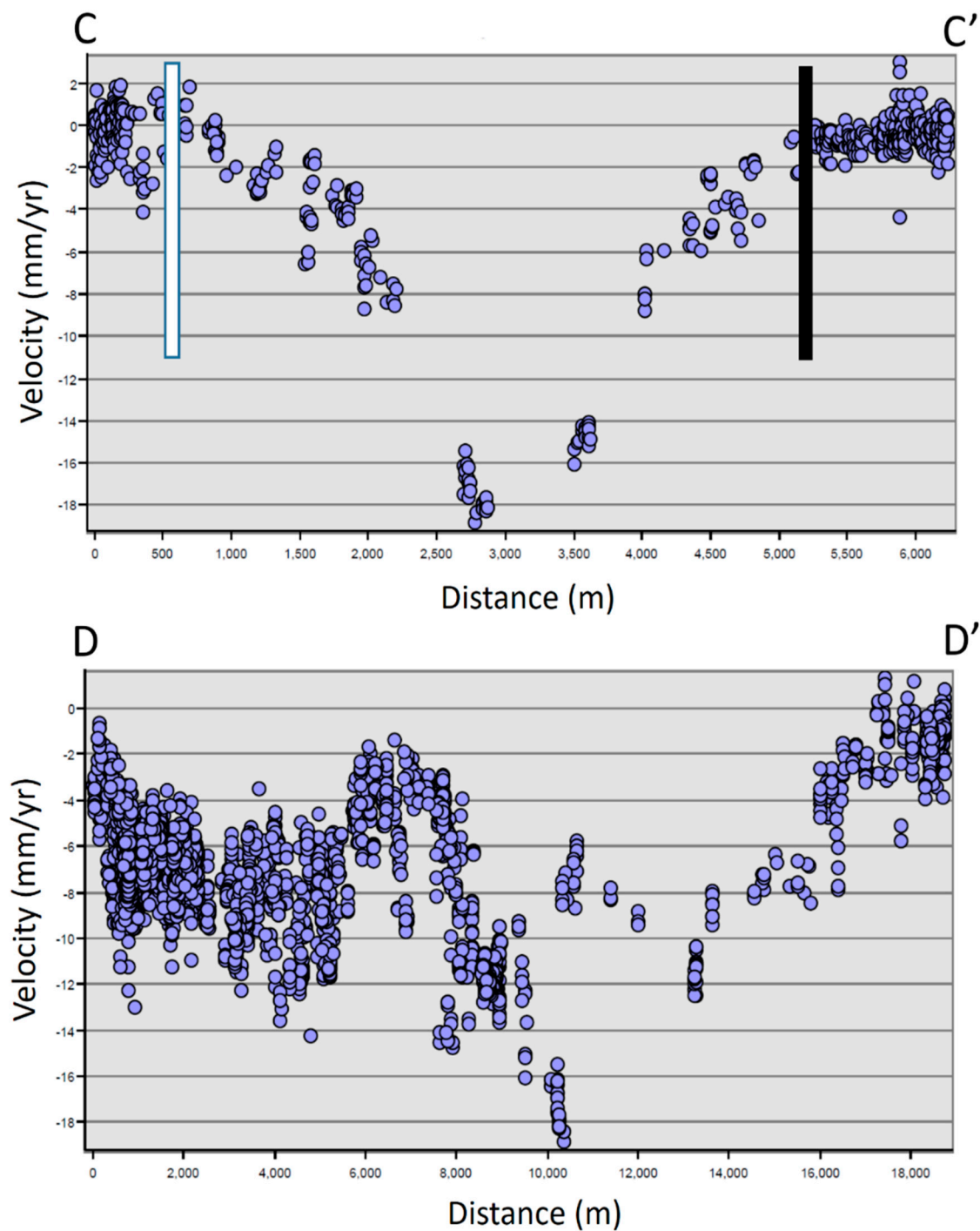


Figure 17. Cont.



**Figure 17.** Graphs are the PSI velocity profiles (shown with green lines at the top map) of the Anthemountas graben. The vertical white and black lines in the graphs indicate the faults, as they appear at the top map.

An important infrastructure located at the Anthemountas graben is the International Airport of Thessaloniki (cyan rectangle Figure 15). It is shown here that during the monitoring period, the airport has a subsidence signal reaching  $-12$  mm/yr (Figure 16). This is located at the intersection of the two airport runways. The current terminal of the airport was found to have been subsiding with a rate of  $-8$  mm/yr, during 2015–2019.

### 3.4. Nea Moudania

Nea Moudania plain drew the attention of the researchers for the first time, due to recently occurring deformation pattern identified at the site. The wider region belongs to the Paeonian subzone, part of the Axios geotectonic zone. The Litho-stratigraphy of the study area is divided into the following formations [47,48].

Quaternary formations, located mainly near the coastal areas, including alluvial deposits (sands, clay), coastal deposits (beach ridges etc.), lagoon deposits (sands, clayey sand), and alluvial fans (Figure 18). Furthermore, along the streams, two terrace systems can be identified. The lower consists mainly of sands, schists, and limestone pebbles and the upper of metamorphic rock pebbles. Neogene formations cover the pre-Neogene bedrock formations. They can be distinguished into the lower red clays series, occupying most of the study area and the upper marls with sandstone series, outcropping at the west of the study area. The red clays series consists mainly of red silty clays with fine-grained quartz and mica, intercalated by sand, marl, and conglomerate lances. The marl with sandstone series consists of altering beds of sand, clay, and clay-marl. Regarding the bedrock, it consists of partly recrystallized bluish limestone, greenish-brown two mica gneiss, and muscovite gneiss.

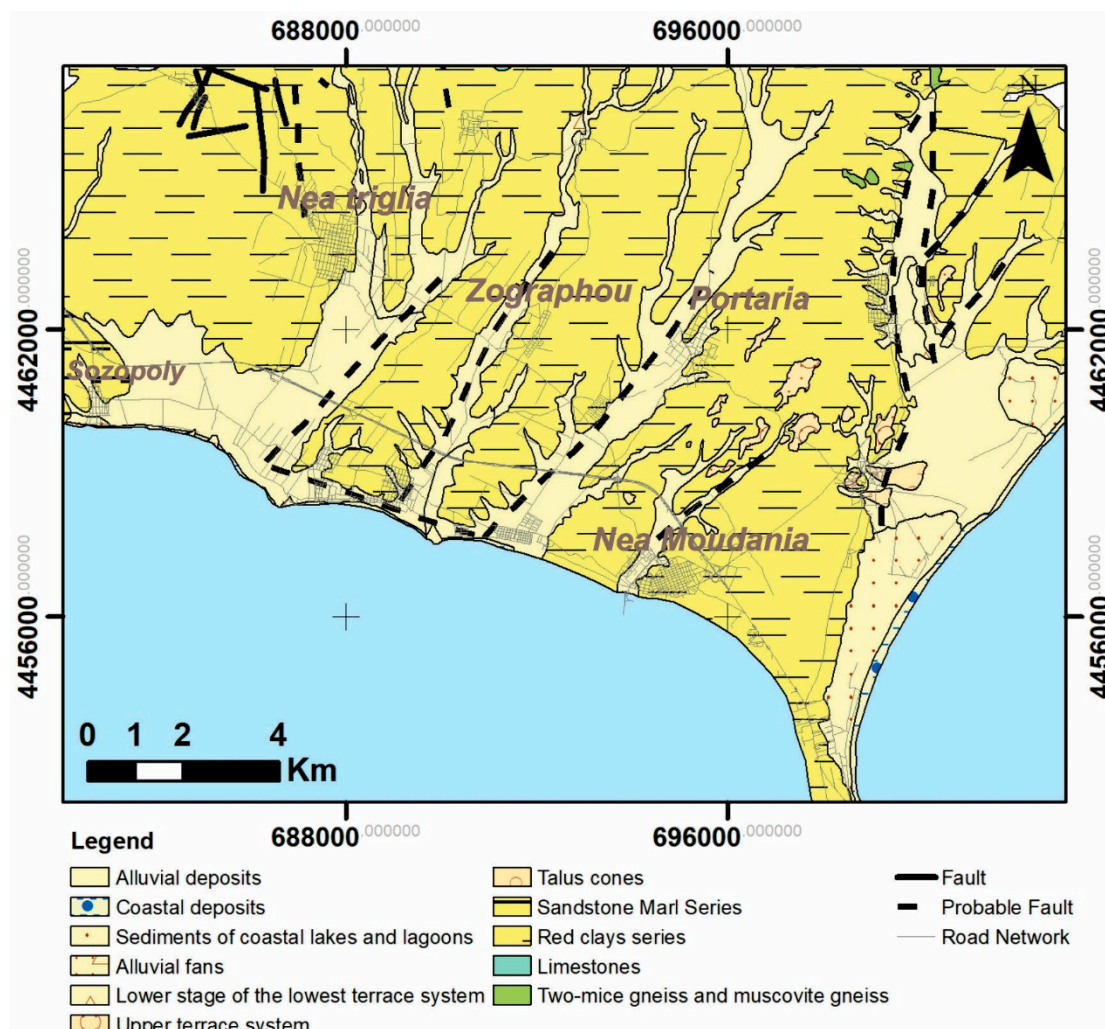


Figure 18. Geological map of Nea Moudania.

Two aquifer systems can be identified at the study area: a shallow unconfined aquifer and a deep confined aquifer [49]. The shallow phreatic aquifer mainly occupies the alluvial Quaternary deposits and the deep confined aquifer the permeable strata intercalated into the Neogene formations,

namely sand, conglomerate, and sandstone layers. The confined aquifer system’s thickness exceeds 200 m in depth [50]. The water provided laterally by the karstic aquifers of the bedrock formations, as well as the water infiltrated from the streams and the precipitation, are the main sources of water for the aquifers.

The Sentinel-1 based PSI results indicate a significant surface displacement (Figure 19). The subsidence rates have a maximum value of -23 mm/yr, during the time span of 2015–2019.

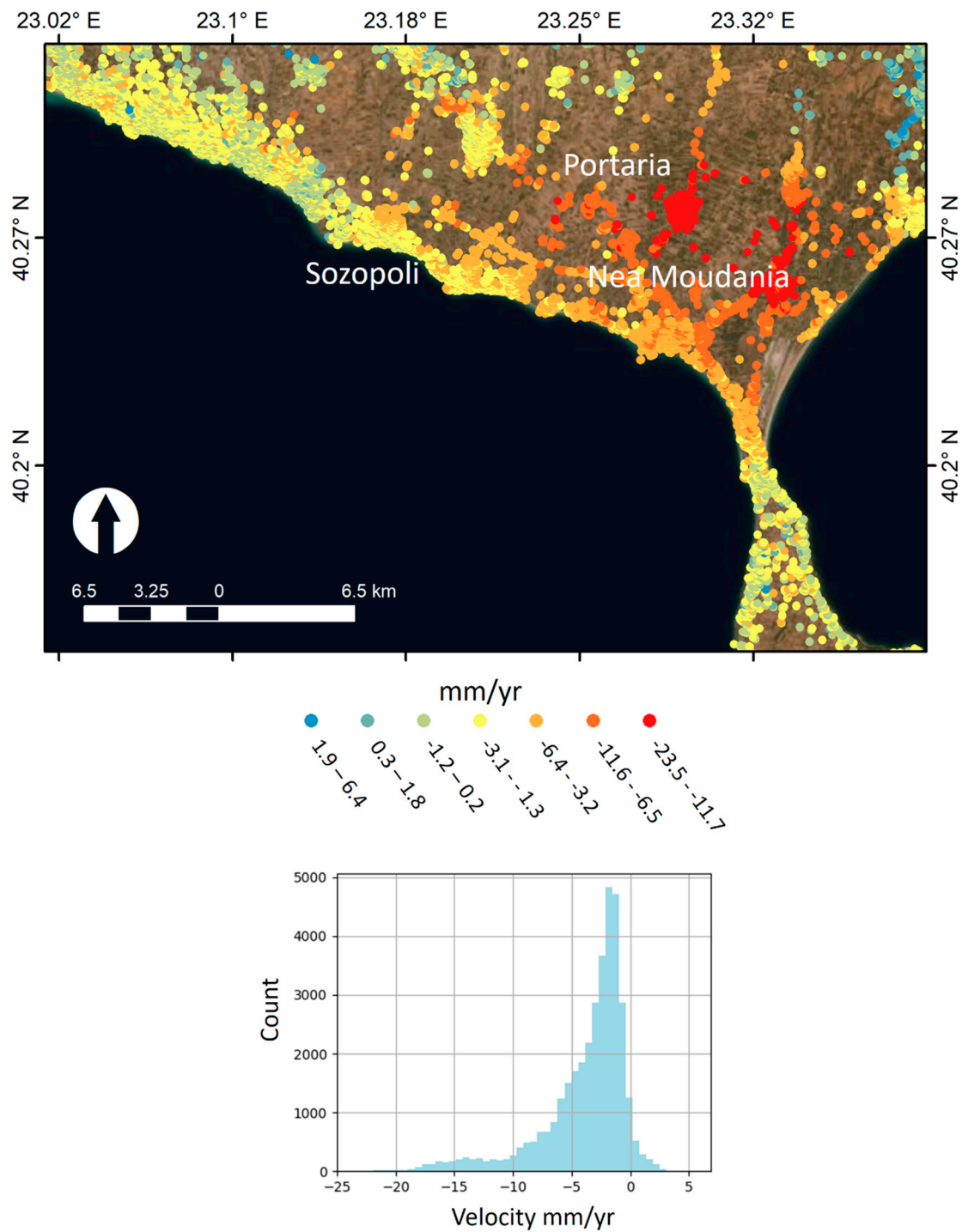
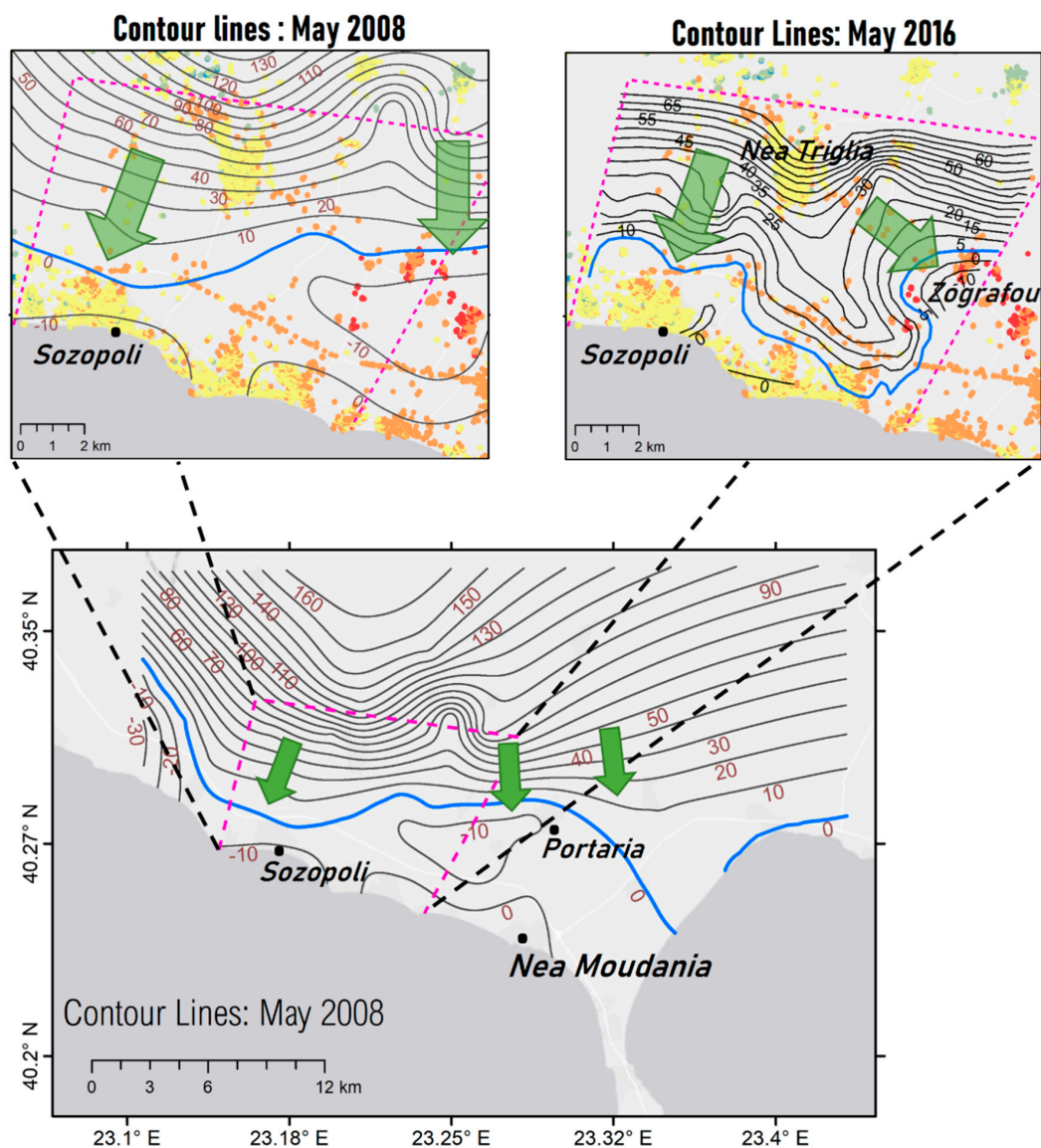


Figure 19. PS velocity map in the broader area of Nea Moudania.

The small extent of the alluvial deposits, in combination with the overexploitation of the shallow aquifer over the past decades has led to the draining of the phreatic aquifer [51]. Since the 1990s,

numerous deep wells have been constructed in the area to meet the water needs [52]. The confined aquifer system of the Neogene formations is considered to be the main source of underground water.

According to data provided by Veranis and Xatzikirkou [50] during the late 2000s, the distribution of the piezometric lines have been clearly indicating the initiation of a sea water intrusion, along the coastal area close to Sozopoly, as well as a depression cone at the plane area NW of Nea Moudania town, both due to the overexploitation of the aquifers (Figure 20). The depression cone had been covering the plane area extending up to the north close to Portaria and Zographou villages with a maximum depression of approximately -15 m. According to the 2016 data provided by Gavrihliou [53], since 2008 the conditions radically changed. The zero level contour line (blue line in Figure 20) moved half way towards Nea Triglia village and the depression cone extended much more to the NW including clearly Portaria and Zographou villages (Figure 18).



**Figure 20.** The confined aquifer piezometric contour lines of the broader area of Nea Moudania. Map at the bottom refers to May 2008 [50]. The magenta dashed rectangle is also shown enlarged in the two inset maps, where the differences between May 2008 and May 2016—modified by the authors from [53]—contour patterns can be compared together also with the PS velocities. Blue line is the 0-level contour line. Water flow is indicated by Green arrows.

Unluckily, the available groundwater level data referring to 2016, do not allow the production of piezometric curves covering the same area with the one covered by the 2008 data, but nevertheless an expansion of the depression cone is clearly evident (Figure 20). Also, the changes observed in the flow direction of the ground water prove the expansion of the depression cone. As shown from the comparisons of the two upper inset maps in Figure 20 (Contours May 2008 and May 2016), the flow direction heading to the sea during 2008 changed by turning to a SE flow, towards the center of the plane area. As the extent of the depression cone coincides with the spatial distribution of the PS indicating subsidence, it can be inferred that the deformations are connected with the consolidation of the formations, triggered by the overexploitation of the aquifer.

#### 4. Discussion

In all cases presented, the detected surface displacements are mainly related to the trends of the hydraulic head. During the recharge of the underground water level, there is an increase of the pore fluid pressure and a decrease of the effective stresses. This is the period where we can have a surface uplift, like for example the one identified in Oreokastro during the 2000s and also from ~2015 to 2019 or like in Kalochori–Sindos during the 2000s. On the contrary, a decrease of the groundwater level causes an increase of the effective stresses and as a result, subsidence. As identified by the InSAR studies this was occurring at Kalochori–Sindos during the 1990s and from ~2015 to 2019, in Oreokastro during the 1990s and in Athemountas during 1990s, 2000s, and during the period of 2015–2019.

In several areas around the world artificial aquifer recharge strategies are followed aiming to overcome the subsidence phenomena. It has been shown that at least for the areas of Oreokastro and Kalochori–Sindos, the surface rebound and the return to a non-deforming state, can be achieved naturally. This could potentially be the result of the generation of rational water management. However, if the groundwater decline continues, the subsidence will continue and the failures will be ongoing in the future. Even though significant hazards have occurred at those areas, the detected natural recharge is a positive factor to be taken into account; at those areas, there is still a regime of rebound deformation. If at some point the underground water level decrease becomes severe enough to cause stresses that exceed the preconsolidation stresses, a rearrangement of the granular material of the aquitards could occur. Then, the area will start experiencing inelastic deformation (e.g., [54–58]). In this case, the results would be irreversible or only partially reversible, even in the case of an aquifer recharge [59].

#### 5. Conclusions

Based on Sentinel-1 and new in-situ underground water level data, we analyzed several areas in the broader area of the city of Thessaloniki, which were found to be deforming during the years of 2015–2019. For the area of Kalochori–Sindos, even though there was a natural rebound after 2000—pausing the subsidence rates of the past—this study showed that a clear subsidence trend has been initiated again. It also became clear that the surface of the area is very sensitive to the changes of the aquifer trends. Moreover, the study shows that the broader area of Oreokastro is still uplifting since the pause of its subsidence trend that occurred after the 1990s. The groundwater level activity enabled us to see discontinuities whose nature and cause could be related to tectonic or other types of geological structures. At this stage, we consider that a geophysical survey at Oreokastro might provide additional insights. The displacement of Anthemountas basin is still ongoing, with the same magnitude as the values detected during the 2000s. Another important fact presented here is that the displacement trend still continues throughout the entire basin and not only on the coastal part of Anthemountas. Significant subsidence occurs also at the area of the International Airport of Thessaloniki where as before, a continuous monitoring seems necessary. A new area that was found for the first time to be affected by subsidence is the Nea Moudania plain. Our analysis highlights that it is also attributed to an anthropogenically derived hazard, linked with water overpumping.

Since most of the study areas presented here have been deforming, occasionally with different trends, for at least ~25 years, it becomes clear that a water management plan should be a forefront priority in the agenda of the decision makers.

**Supplementary Materials:** The following are available online at <http://www.mdpi.com/2072-4292/12/15/2396/s1>, Figure S1: Standard deviation of the PS S-1 results.

**Author Contributions:** Conceptualization, N.S., C.L., I.P., and C.K.; formal analysis, S.A., I.P., C.T., N.S.; data curation, P.T., T.S., S.A., I.P., C.T., N.S.; writing—original draft preparation, N.S., C.L.; writing—review and editing, C.L., I.P., C.K., S.A., C.T.; T.S.; visualization, N.S., C.L., I.P., S.A.; funding acquisition, C.K. All authors have read and agreed to the published version of the manuscript.

**Funding:** This research was supported by the Next Generation GEOSS for Innovation Business (NextGEOSS), European Commission, grant agreement ID 730329.

**Acknowledgments:** European Space Agency and Copernicus EU are thanked for the provision of Sentinel-1 images. Hydrogeological data for Kalochori–Sindos is a courtesy of the Water Supply and Sewerage Company of Thessaloniki (EYATH). The faults are from Zervopoulou (2010) and the NOA fault database (Ganas et al. 2013). The authors would like to thank Tree-Company and Dionysos Satellite Observatory of National Technical University of Athens for providing GPS velocities for VRAS station.

**Conflicts of Interest:** The authors declare no conflict of interest.

## References

- Loupasakis, C.; Angelitsa, V.; Rozos, D.; Spanou, N. Mining geohazards—Land subsidence caused by the dewatering of opencast coal mines: The case study of the Amyntaio coal mine, Florina, Greece. *Nat. Hazards* **2013**, *70*, 675–691. [[CrossRef](#)]
- Psimoulis, P.; Ghilardi, M.; Fouache, E.; Stiros, S. Subsidence and evolution of the Thessaloniki plain, Greece, based on historical leveling and GPS data. *Eng. Geol.* **2007**, *90*, 55–70. [[CrossRef](#)]
- Galloway, D.L.; Hoffmann, J. The application of satellite differential SAR interferometry-derived ground displacements in hydrogeology. *Hydrogeol. J.* **2006**, *15*, 133–154. [[CrossRef](#)]
- Lu, Z.; Danskin, W.R. InSAR analysis of natural recharge to define structure of a ground-water basin, San Bernardino, California. *Geophys. Res. Lett.* **2001**, *28*, 2661–2664. [[CrossRef](#)]
- Alatza, S.; Papoutsis, I.; Paradissis, D.; Kontoes, C.; Papadopoulos, G.A. Multi-Temporal InSAR Analysis for Monitoring Ground Deformation in Amorgos Island, Greece. *Sensors* **2020**, *20*, 338. [[CrossRef](#)]
- Triantafyllou, A.I.; Vergos, G.S.; Tziavos, I.N. Contribution of Sentinel-1 Dinsar to the Determination of Vertical Deformation and Height System Monitoring. In Proceedings of the 4th Joint International Symposium on Deformation Monitoring (JISDM), Athens, Greece, 15–17 May 2019.
- Papoutsis, I.; Kontoes, C.; Paradissis, D. Multi-Stack Persistent Scatterer Interferometry Analysis in Wider Athens, Greece. *Remote Sens.* **2017**, *9*, 276. [[CrossRef](#)]
- Foumelis, M.; Papageorgiou, E.; Stamatopoulos, C.A. Episodic ground deformation signals in Thessaly Plain (Greece) revealed by data mining of SAR interferometry time series. *Int. J. Remote Sens.* **2016**, *37*, 3696–3711. [[CrossRef](#)]
- Mouratidis, A.; Briole, P.; Ilieva, M.; Astaras, T.; Rolandone, F.; Baccouche, M. Subsidence and deformation phenomena in the vicinity of Thessaloniki (N. Greece) monitored by Envisat/ASAR interferometry. In Proceedings of the Fringe 2009 Workshop: “Advances in the Science and Applications of SAR Interferometry”, Frascati, Italy, 30 November–4 December 2009.
- Raucoules, D.; Parcharidis, I.; Feurer, D.; Novalli, F.; Ferretti, A.; Carnec, C.; Lagios, E.; Sakkas, V.; Le Mouélic, S.; Cooksley, G.; et al. Ground deformation detection of the greater area of Thessaloniki (Northern Greece) using radar interferometry techniques. *Nat. Hazards Earth Syst. Sci.* **2008**, *8*, 779–788. [[CrossRef](#)]
- Svigkas, N.; Papoutsis, I.; Loupasakis, C.; Kontoes, C.; Kiratzi, A. Geo-hazard Monitoring in Northern Greece Using InSAR techniques: The case Study of Thessaloniki. In *Proceedings of Fringe 2015: Advances in the Science and Applications of SAR Interferometry and Sentinel-1 InSAR Workshop*; European Space Agency: Paris, France, 2015.
- Raspini, F.; Loupasakis, C.; Rozos, D.; Moretti, S. Advanced interpretation of land subsidence by validating multi-interferometric SAR data: The case study of the Anthemountas basin (Northern Greece). *Nat. Hazards Earth Syst. Sci.* **2013**, *13*, 2425–2440. [[CrossRef](#)]

13. Raspini, F.; Loupasakis, C.; Rozos, D.; Adam, N.; Moretti, S. Ground subsidence phenomena in the Delta municipality region (Northern Greece): Geotechnical modeling and validation with Persistent Scatterer Interferometry. *Int. J. Appl. Earth Obs. Geoinf.* **2014**, *28*, 78–89. [[CrossRef](#)]
14. Svigkas, N.; Papoutsis, I.; Loupasakis, C.; Tsangaratos, P.; Kiratzi, A.; Kontoes, C.H. Land subsidence rebound detected via multi-temporal InSAR and ground truth data in Kalochori and Sindos regions, Northern Greece. *Eng. Geol.* **2016**, *209*, 175–186. [[CrossRef](#)]
15. Svigkas, N.; Papoutsis, I.; Loupasakis, C.; Tsangaratos, P.; Kiratzi, A.; Kontoes, C.H. InSAR time-series monitoring of ground displacement trends in an industrial area (Oreokastro—Thessaloniki, Greece): Detection of natural surface rebound and new tectonic insights. *Environ. Earth Sci.* **2017**, *76*. [[CrossRef](#)]
16. Svigkas, N.; Papoutsis, I.; Loupasakis, C.; Tsangaratos, P.; Kiratzi, A.; Kontoes, C.H. Radar Space Measurements of the Deforming Trends at Northern Greece Resulting from Underground Water Activity. In *Advances in Remote Sensing and Geo Informatics Applications*; Springer International Publishing: Cham, Switzerland, 2019; pp. 309–313.
17. Svigkas, N.; Loupasakis, C.; Tsangaratos, P.; Papoutsis, I.; Kiratzi, A.; Kontoes, C.H. A deformation study of Anthemountas graben (northern Greece) based on in situ data and new InSAR results. *Arab. J. Geosci.* **2020**, *13*, 1–13. [[CrossRef](#)]
18. Galloway, D.L.; Hudnut, K.W.; Ingebritsen, S.E.; Phillips, S.P.; Peltzer, G.; Rogez, F.; Rosen, P.A. Detection of aquifer system compaction and land subsidence using interferometric synthetic aperture radar, Antelope Valley, Mojave Desert, California. *Water Resour. Res.* **1998**, *34*, 2573–2585. [[CrossRef](#)]
19. Papoutsis. InSAR Greece: A national ground motion service, based on big Copernicus Sentinel-1 data. *Remote Sens.* **2020**. under review.
20. Fattahi, H.; Agram, P.; Simons, M. A Network-Based Enhanced Spectral Diversity Approach for TOPS Time-Series Analysis. *IEEE Trans. Geosci. Remote Sens.* **2016**, *55*, 777–786. [[CrossRef](#)]
21. Hooper, A.; Zebker, H.; Segall, P.; Kampes, B. A new method for measuring deformation on volcanoes and other natural terrains using InSAR persistent scatterers. *Geophys. Res. Lett.* **2004**, *31*, L23611. [[CrossRef](#)]
22. Hooper, A.; Segall, P.; Zebker, H. Persistent scatterer interferometric synthetic aperture radar for crustal deformation analysis, with application to Volcán Alcedo, Galápagos. *J. Geophys. Res. Space Phys.* **2007**, *112*, B07407. [[CrossRef](#)]
23. Farr, T.G.; Kobrick, M. Shuttle radar topography mission produces a wealth of data. *Eos Trans. Am. Geophys. Union* **2000**, *81*, 583–585. [[CrossRef](#)]
24. Bekaert, D.; Walters, R.; Wright, T.J.; Hooper, A.; Parker, D.J. Statistical comparison of InSAR tropospheric correction techniques. *Remote Sens. Environ.* **2015**, *170*, 40–47. [[CrossRef](#)]
25. Hatzinakos, I.; Rozos, D.; Apostolidis, E. Engineering geological mapping and related geotechnical problems in the wider industrial area of Thessaloniki, Greece. In *International Congress International Association of Engineering Geology*; Price, D., Ed.; A. A. Balkema: Rotterdam, The Netherlands, 1990; pp. 127–134.
26. Rozos, D.; Apostolidis, E.; Christaras, B. Engineering-geological map of Thessaloniki wider area. *Bull. Eng. Geol. Environ.* **2004**, *63*, 103–108.
27. Loupasakis, C.; Rozos, D. Land subsidence induced by the overexploitation of the aquifers in Kalochori village—New approach by means of the computational geotechnical engineering. *Bull. Geol. Soc. Greece* **2010**, *43*, 1219–1229. [[CrossRef](#)]
28. IGME Institute of Geological and Mineralogical Exploration. *Geological Map of Greece, Scale 1:50,000*; Thessaloniki Sheets; IGME: Athens, Greece, 1978.
29. Andronopoulos, V.; Rozos, D.; Hatzinakos, J. *Geotechnical Study of Ground Settlement in the Kalochori Area, Thessaloniki District*; Unpublished Report; IGME: Athens, Greece, 1990; p. 45.
30. Rozos, D.; Hatzinakos, I. Geological conditions and geomechanical behaviour of the neogene sediments in the area west of Thessaloniki (Greece). In *Geotechnical Engineering of Hard Soils-Soft Rocks*; A.A. Balkema: Rotterdam, The Netherlands, 1993; pp. 269–274.
31. Stiros, S. Subsidence of the Thessaloniki (northern Greece) coastal plain, 1960–1999. *Eng. Geol.* **2001**, *61*, 243–256. [[CrossRef](#)]
32. Loupasakis, C.; Rozos, D. Land subsidence induced by water pumping in Kalochori village (North Greece) —Simulation of the phenomenon by means of the finite element method. *Q. J. Eng. Geol. Hydrogeol.* **2009**, *42*, 369–382. [[CrossRef](#)]



33. Ganas, A.; Chousianitis, K.; Argyrakis, P.; Tsimi, C.; Papanikolaou, M.; Papathanassiou, G.; Exarchos, K. Monitoring of Surface Displacements in the Kalochori Area (Thessaloniki, Greece) Using a Local Gns Network. *Bull. Geol. Soc. Greece* **2017**, *50*, 1553–1562. [[CrossRef](#)]
34. Zervopoulou, A. Neotectonic Faults in the Broader Area of Thessaloniki, in Relation to the Foundation Soils. Ph.D. Thesis, Aristotle University of Thessaloniki, Thessaloniki, Greece, 2010.
35. Papazachos, C.; Soupios, P.; Savvaidis, A.; Roumelioti, Z. Identification of small-scale active faults near metropolitan areas: An example from the Asvestochori fault near Thessaloniki. In Proceedings of the XXXII ESC General Assembly 2000, Lisbon, Portugal, 10–15 September 2000; pp. 221–225.
36. Paradisopoulou, P.M.; Karakostas, V.G.; Papadimitriou, E.E.; Tranos, M.D.; Papazachos, C.B.; Karakaisis, G.F. Microearthquake study of the broader Thessaloniki area (Northern Greece). *Ann. Geophys.* **2006**, *49*, 1081–1093.
37. Garlaouni, C.; Papadimitriou, E.; Karakostas, V.; Kiliadis, A.; Lasocki, S. Fault population recognition through microseismicity in Migdonia region (northern Greece). *Boll. Geofis. Teor. Appl.* **2015**, *56*, 367–382.
38. European Center on Prevention and Forecasting of Earthquakes (ECPFE). *Earthquake Planning and Protection Organization (EPPO) & Tectonic Committee of the Geological Society of Greece 1996 Neotectonic Map of Greece, Thessaloniki Sheet, Scale: 1:100000*; EPPO & ECPFE: Athens, Greece, 1996.
39. Ganas, A.; Oikonomou, I.A.; Tsimi, C. NOA faults: A digital database for active faults in Greece. *Bull. Geol. Soc. Greece* **2017**, *47*, 518. [[CrossRef](#)]
40. Fikos, I.; Ziankas, G.; Rizopoulou, A.; Famellos, S. Water balance estimation in Anthemountas river basin and correlation with underground water level. *Glob. NEST J.* **2005**, *7*, 354–359.
41. ZEPBOIIOYΛOY, A.; ΠΑΥΛΙΔΗΣ, Σ. Morphotectonic Study of the Broader Area of Thessaloniki for the Cartography of Neotectonic Faults. *Bull. Geol. Soc. Greece* **2005**, *38*, 30–41. [[CrossRef](#)]
42. Rozos, D.; Hatzinakos, I.; Apostolidis, E. *Engineering Geological Map of Thessaloniki Wider Area*; Scale 1:25,000; Institute of Geological and Mineralogical Exploration I.G.M.E.: Athens, Greece, 1998.
43. Thanasoulas, K. *Geophysical Study of Anthemountas Area*; Technical Report Institute of Geological and Mineralogical Exploration IGME: Athens, Greece, 1983. (In Greek)
44. Anastasiadis, A.; Raptakis, D.; Ptilakis, K. Thessaloniki's Detailed Microzoning: Subsurface Structure as Basis for Site Response Analysis. *Pure Appl. Geophys. PAGEOPH* **2001**, *158*, 2597–2633. [[CrossRef](#)]
45. Nagoulis, A.; Loupasakis, C. Hydrogeological conditions of the plain area of the Anthemounta basin (Macedonia, Greece). *Bull. Geol. Soc. Greece* **2001**, *34*, 1859–1868.
46. IGME Institute of Geological and Mineralogical Exploration. *Geological Map Sheets, Scale 1:50,000*; Epanomi (1969), Thessaloniki (1978), Thermi (1978) and Vasilika (1978); IGME: Athens, Greece, 1978.
47. Syridis, G. Lithostromatographical, Biostromatographical and Paleostromatographical Study of Neogene-Quaternary Formation of Chalkidiki Peninsula. Ph.D. Thesis, Aristotle University of Thessaloniki, Thessaloniki, Greece, 1990.
48. IGME Institute of Geological and Mineralogical Exploration. *Geological Map of Greece, Scale 1:50,000*; Poliyiros and Vasilika Sheet; IGME: Athens, Greece, 1978.
49. Latinopoulos, P.; Theodossiou, N.; Xeferis, A.; Mallios, Z.; Papageoriou, A.; Fotopoulou, E. *Developing Water Resources Management Plan for Water Supply-Irrigation*; Final Research Project; Aristotle University of Thessaloniki: Thessaloniki, Greece, 2003.
50. Veranis, N.; Xatzikirkou, A. *Hydrogeological Report Central Macedonia. Aquifers of Epanomis-Moudaniwn, Kassandras, Ormilias and Sithonias*; Unpublished technical report; IGME: Thessaloniki, Spain, 2010; p. 394.
51. Siarkos, I. Developing a Methodological Framework Using Mathematical Simulation Models in Order to Investigate the Operation of Coastal Aquifer Systems: Application in the Aquifer of N. Moudania. Ph.D. Thesis, Aristotle University of Thessaloniki, Thessaloniki, Greece, 2015.
52. Xeferis, A. Investigating the Deterioration of Groundwater in “Kalamaria Plain” Emphasizing on Nitrates. Ph.D. Thesis, Civil Engineering Department, Aristotle University of Thessaloniki, Thessaloniki, Greece, 2000.
53. Gavrihidou, E. The Long Term Study of the Variability of Hydrological Parameters and their Impacts on Groundwater Reserves at Coastal Aquifers. Master's Thesis, Geological Department, Aristotle University of Thessaloniki, Thessaloniki, Greece, 2017.
54. Haghghi, M.H.; Motagh, M. Ground surface response to continuous compaction of aquifer system in Tehran, Iran: Results from a long-term multi-sensor InSAR analysis. *Remote Sens. Environ.* **2019**, *221*, 534–550. [[CrossRef](#)]

55. Galloway, D.L.; Burbey, T.J. Review: Regional land subsidence accompanying groundwater extraction. *Hydrogeol. J.* **2011**, *19*, 1459–1486. [[CrossRef](#)]
56. Hoffmann, J.; Zebker, H.A.; Galloway, D.L.; Amelung, F. Seasonal subsidence and rebound in Las Vegas Valley, Nevada, observed by Synthetic Aperture Radar Interferometry. *Water Resour. Res.* **2001**, *37*, 1551–1566. [[CrossRef](#)]
57. Helm, D.C. One-dimensional simulation of aquifer system compaction near Pixley, California: 1. Constant parameters. *Water Resour. Res.* **1975**, *11*, 465–478. [[CrossRef](#)]
58. Helm, D.C. One-dimensional simulation of aquifer system compaction near Pixley, California: 2. Stress-Dependent Parameters. *Water Resour. Res.* **1976**, *12*, 375–391. [[CrossRef](#)]
59. Schmidt, D.A.; Bürgmann, R. Time-dependent land uplift and subsidence in the Santa Clara valley, California, from a large interferometric synthetic aperture radar data set. *J. Geophys. Res. Space Phys.* **2003**, *108*, 2416. [[CrossRef](#)]



© 2020 by the authors. Licensee MDPI, Basel, Switzerland. This article is an open access article distributed under the terms and conditions of the Creative Commons Attribution (CC BY) license (<http://creativecommons.org/licenses/by/4.0/>).